International Journal of Fracture **125:** 1–32, 2004.

Crack tunneling and plane-strain delamination in layered solids

AKKE S.J. SUIKER[1] and NORMAN A. FLECK[2]
[1]*Delft University of Technology, Koiter Institute Delft / Faculty of Aerospace Engineering, P.O. Box 5058, 2600 GB DELFT, The Netherlands.*
[2]*Cambridge University, Cambridge Centre for Micromechanics / Department of Engineering, Trumpington Street, CAMBRIDGE, CB2 1PZ, U.K.*

Received 15 July 2003; accepted in revised form 5 December 2003

Abstract. Steady-state tunneling and plane-strain delamination of an H-shape crack are examined for elastic, isotropic multi-layers. Both tunneling and delamination are analysed by employing linear elastic fracture mechanics within a 2D finite element framework. Failure maps are produced to reveal the sensitivity of cracking path to the relative toughness of layer and interface, and to the stiffness mismatch of layers. Closed-form expressions are derived for the critical stress level for steady-state plane-strain delamination. By means of a comparison with experimental results taken from the literature, it is demonstrated that these expressions serve as useful design criteria for elastic multilayers.

Key words: Bi-materials, failure mechanisms, fibre-reinforced laminates, GLARE, H-shape crack.

1. Introduction

The fatigue and fracture behaviour of fibre-metal laminates and fibre-reinforced ceramic-matrix composites is of current technological interest because of the increasing number of applications enjoyed by these materials in aerospace engineering, transport industry and general engineering. A typical laminate structure is an alternating stack of aluminium alloy sheets and fibre-reinforced epoxy layers. Laminates reinforced by aramid and glass fibres are commercially known as ARALL and GLARE, respectively, and have been extensively tested over the past 15 years (Marissen, 1988; Vermeeren, 1995; Vogelesang et al., 1995; Vlot et al., 1999; Takamatsu et al., 1999; de Vries et al., 1999; de Vries, 2001; Vlot and Gunnink, 2001). It has been found experimentally that these laminates are fatigue-resistant since the fibre-epoxy layers arrest the transverse growth of a mode I crack in the metal layer, see Figure 1. Instead, the crack tunnels as shown.

In order to activate the mechanism depicted in Figure 1, it is essential that the initial mode I crack within the mid-layer does not penetrate the fibre layer when it reaches the interface, but rather kinks along the interface to give interfacial delamination. He and Hutchinson (1989) have developed criteria for the possible kinking of a mode I crack at a brittle interface between dissimilar elastic solids. They argued that the competition between delamination and crack penetration is governed by the ratio of energy release rate for crack deflection into the delamination plane, G_d, and the energy release rate for continued mode I crack penetration into the fibre/epoxy layer, G_{Ip}. Upon denoting the toughness for (mixed-mode) delamination as G_{dc}, and the toughness for mode I crack penetration in the fibre/epoxy layer as G_{Ipc}, delamination is predicted when

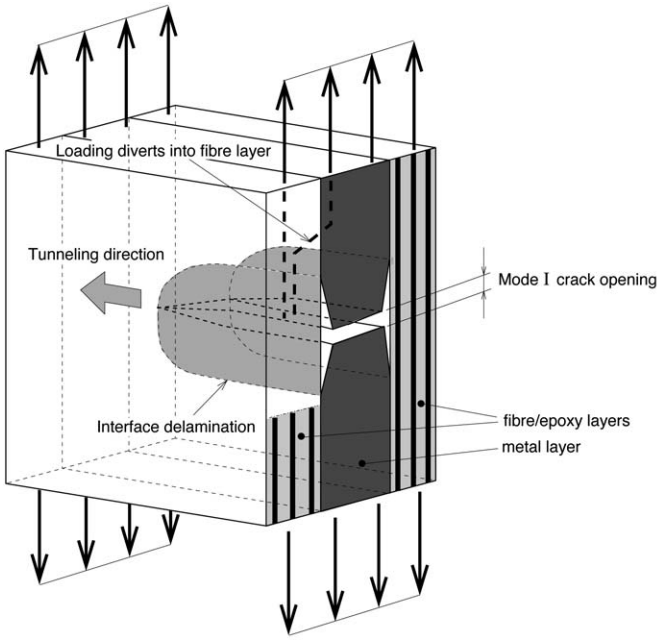

Figure 1. H-shape crack tunneling in a fibre-metal laminate.

$$\frac{G_d}{G_{Ip}} > \frac{G_{dc}}{G_{Ipc}}. \tag{1}$$

Conversely, the mode I crack penetrates the fibre/epoxy layer without kinking when the inequality sign in Equation (1) is reversed. Thus, when delamination precedes penetration, the Griffith fracture criterion is $G_d = G_{dc}$, where the subscript c denotes 'critical'; alternatively, when crack penetration of the interface precedes delamination the Griffith fracture criterion is $G_{Ip} = G_{Ipc}$.

Over the last two decades, the mechanics of crack branching at an interface between two dissimilar materials has been studied for various geometries. An extensive overview of studies on interface delamination can be found in Hutchinson and Suo (1992). For the specific case of a layer sandwiched between two substrates, mode I cracking in the layer combined with symmetric delamination along the interfaces with the substrates leads to an H-shape crack pattern, as sketched in Figure 1. Dollar and Steif (1991a) have studied the mechanics of an H-shape crack in a homogeneous, isotropic, infinite medium subjected to a remote tensile stress, and Lu (1996) has extended this analysis by accounting for the effect of residual stress caused by a thermal expansion mismatch. Chan et al. (1993) investigated an H-shape crack in an infinite homogeneous medium by including the influence of plastic yielding at the delamination planes. The growth of a periodic array of identical H-shape cracks in an infinite homogeneous medium, with delamination obeying a Coulomb friction law, has been addressed by Dollar and Steif (1991b).

The current study considers possible crack propagation paths for alternating layers of two dissimilar but isotropic elastic, brittle solids, designated as materials '1' and '2' in Figure 2. The initiation/nucleation phase of cracking is neglected, and it is assumed that the crack has grown from a large pre-existing flaw in the mid-layer (material 1). The competition is addressed for: (i) tunneling of a mode I crack in the mid-layer with delamination absent (*mech-*

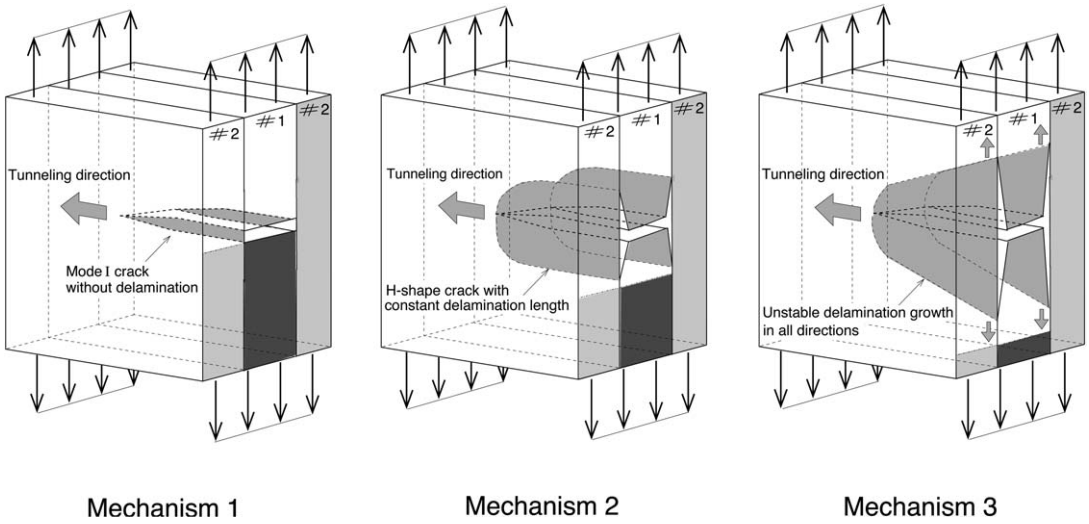

Figure 2. Three possible failure mechanisms for a laminate of two dissimilar, isotropic materials. *Mechanism 1*: Tunneling of a mode I crack without delamination. *Mechanism 2*: Tunneling of an H-shape crack with constant delamination length. *Mechanism 3*: Unstable delamination growth in all directions.

anism 1), (ii) tunneling of an H-shape crack with constant delamination length (*mechanism 2*), and (iii) unstable delamination in all directions (*mechanism 3*). Failure mechanism maps are constructed to reveal the sensitivity of the operative cracking mechanism to the relative toughness of layer and interface, and to the stiffness mismatch of the layers. Additionally, the dependence of fracture strength upon crack location and laminate thickness are explored.

In Cox and Marshall (1996), three failure mechanisms analogous to those in Figure 2 were derived for a mode I transverse ply crack in a laminated ceramic composite. Instead of considering delamination, they assumed that the transverse ply crack penetrates the adjacent fibre layer. In the present study, it is assumed throughout that the penetration toughness G_{Ipc} of the layers adjacent to the H-shape crack is sufficiently high for the crack not to penetrate them (i.e. Equation (1) is assumed to hold); this is commonly the case for the laminates ARALL and GLARE (Marissen, 1988; de Vries, 2001; Vlot and Gunnink, 2001). The assumption of elastic isotropy may be an acceptable simplification for multi-directional fibrous laminates when the elastic mismatch between fibres and matrix is moderate. The significance of material anisotropy upon the cracking pattern must await a later study.

Both plane-strain delamination of an H-shape crack and steady state tunneling of an H-shape crack are investigated herein by 2D finite element analyses. Although tunneling is a 3D phenomenon, the remote stress for steady-state tunneling can be computed from a plane-strain elasticity solution for an H-shape crack: the difference in strain energy upstream and downstream of the tunneling crack front is equated to the delamination work and, for simplicity, the delamination toughness G_{dc} is taken to be independent of the mode-mix (Hutchinson and Suo, 1992; Beuth, 1992; Ho and Suo, 1993; Cox and Marshall, 1996; Fleck and Zhao, 2000). This assumption does not introduce large errors: in the present study for all configurations analysed it is found that the mode-mix attains a steady-state value at relatively small delamination lengths.

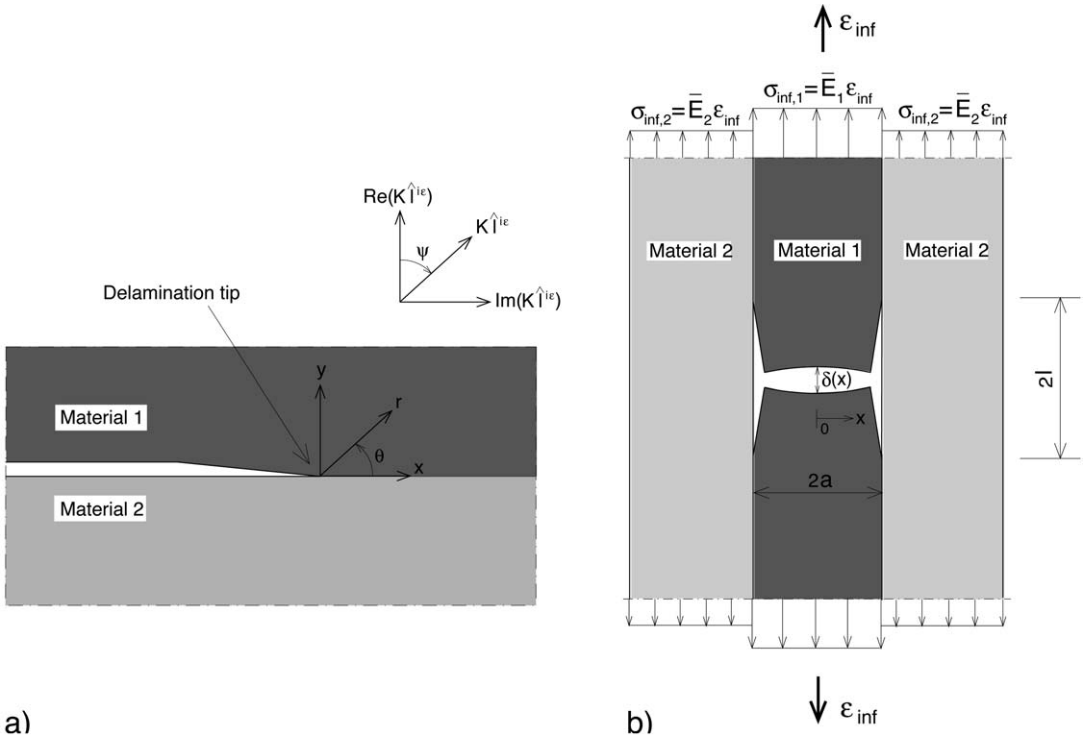

Figure 3. Plane-strain cracking. (a) Delamination along a straight interface between two dissimilar, isotropic materials. The mode-mix of the delamination is indicated by the angle Ψ. (b) H-shape crack as a result of a uniform remote strain ϵ_{inf}.

2. Review of delamination at a bi-material interface

Consider a plane-strain delamination crack along a planar interface between two isotropic but dissimilar materials, as sketched in Figure 3a. The elastic mismatch of the two solids is commonly represented by the Dundurs' parameters α and β (Dundurs, 1969),

$$\alpha = \frac{\bar{E}_1 - \bar{E}_2}{\bar{E}_1 + \bar{E}_2}, \qquad \beta = \frac{1}{2}\frac{(1-2\nu_2)/\mu_2 - (1-2\nu_1)/\mu_1}{(1-\nu_2)/\mu_2 + (1-\nu_1)/\mu_1}, \tag{2}$$

where the subscripts 1 and 2 refer to the solids above and below the interface, respectively, and E is the Young's modulus, ν is the Poisson's ratio and $\mu = E/(2(1+\nu))$ is the shear modulus. The overbar on the Young's modulus denotes the plane-strain value, $\bar{E} \equiv E/(1-\nu^2)$. The parameter α is positive (*negative*) when material 1 is more stiff (*compliant*) than material 2. In the limiting case of a rigid upper layer 1, α attains the value $+1$, while $\alpha = -1$ denotes a rigid lower layer. When the elastic properties of materials 1 and 2 are identical, the parameters α and β both equal zero, and both α and β change sign when the solids above and below the interface are switched.

Generally, the singular stress field at the tip of an interfacial crack is characterised by a *complex stress intensity factor*, $K = K_1 + iK_2$, where $i = \sqrt{-1}$, and K_1 and K_2 are the real and imaginary parts of the stress intensity factor, respectively. The normal stress component σ_{yy} and shear stress component σ_{xy} at a distance r directly ahead of the crack tip are given asymptotically by (Hutchinson et al., 1987; Rice, 1988)

$$\sigma_{yy} + i\,\sigma_{xy} = \frac{K}{\sqrt{2\pi r}} r^{i\varepsilon}, \tag{3}$$

where $r^{i\varepsilon} = e^{i\varepsilon \ln r} = \cos(\varepsilon \ln r) + i \sin(\varepsilon \ln r)$. The parameter ε is the oscillatory index, and is a function of the Dundur's parameter β according to

$$\varepsilon = \frac{1}{2\pi} \ln\left(\frac{1-\beta}{1+\beta}\right). \tag{4}$$

For homogeneous solids and for incompressible bi-materials (i.e. $\nu_1 = \nu_2 = 0.5$), the parameters β and ε vanish, and the oscillatory term $r^{i\varepsilon}$ of Equation (3) becomes unity. Under these circumstances K_1 and K_2 represent the classical mode I and mode II stress intensity factors, and Equation (3) simplifies to $\sigma_{yy} = K_1(2\pi r)^{-1/2}$ and $\sigma_{xy} = K_2(2\pi r)^{-1/2}$.

The oscillatory behaviour introduces a complication to the interpretation of the mode-mix at the delamination tip, which for a crack in a homogeneous solid is defined by $\tan(\psi) = K_2/K_1 = \sigma_{xy}(r)/\sigma_{yy}(r)$ immediately ahead of the crack tip. Rice (1988) extended the classical definition of the mode-mix for the case of an interfacial crack by introducing a reference length $\hat{l}$ such that

$$\tan(\psi) = \frac{\sigma_{xy}\left(r = \hat{l}\right)}{\sigma_{yy}\left(r = \hat{l}\right)} = \frac{\mathrm{Im}(K\hat{l}^{i\varepsilon})}{\mathrm{Re}(K\hat{l}^{i\varepsilon})}. \tag{5}$$

Thus, the mode-mix is defined by the ratio of shear to normal traction on the crack plane immediately ahead of the crack tip, but since this ratio varies with distance r from the crack tip, it is necessary to evaluate this ratio at an arbitrary (but specified) reference length $\hat{l}$ ahead of the crack tip. Fortunately, the particular value taken for $\hat{l}$ has only a small effect upon the value of the phase angle ψ for typical values of ε (Rice, 1988). In the current study the reference length is set equal to the mode I crack semi-width, $\hat{l} = a$ (the reader can relate this choice to a different choice by a simple transformation, as discussed in Rice, 1988). It is noted that Equation (5) reduces to the classical definition for the mode-mix, $\tan(\psi) = K_2/K_1$, when $\beta = \varepsilon = 0$.

The energy release rate per unit crack advance of the interfacial delamination is (Hutchinson and Suo, 1992)

$$G_d = \frac{1-\beta^2}{E_*}(K_1^2 + K_2^2), \tag{6}$$

where $E_* = 2(\bar{E}_1^{-1} + \bar{E}_2^{-1})^{-1}$. An alternative expression for the energy release rate can be obtained by substituting $1 - \beta^2 = 1/\cosh^2(\pi\varepsilon)$ into Equation (6), as noted by Hutchinson et al. (1987) and Rice (1988). As outlined in the introduction, interfacial delamination occurs when the energy release rate, Equation (6), equals the delamination toughness at the appropriate mode-mix,

$$G_d = G_{dc}(\psi(\hat{l})). \tag{7}$$

3. Steady-state tunneling and plane-strain delamination

Consider the case of an H-shape crack tunneling within a symmetric stack of 3 layers as shown in Figure 3b; it is assumed that the tunneling crack has nucleated from a flaw within

material 1 and is driven by a remote load, characterised by a (uniform) tensile strain ε_{inf}, where the subscript 'inf' denotes 'infinity'. The strain level may either represent static or fatigue loading. The Poisson ratios of the materials are assumed to be equal and representative of many fibre-reinforced laminates, $\nu_1 = \nu_2 = 0.3$. The stiffness mismatch is expressed in terms of the ratio of plane-strain stiffness moduli, $\bar{E}_2/\bar{E}_1$, instead of the Dundur's parameters, α, and β. As shown by Equation (2), a direct connection exists between (α, β) and the stiffness ratio $\bar{E}_2/\bar{E}_1$, for $\nu_1 = \nu_2 = 0.3$. As $\bar{E}_2/\bar{E}_1$ ranges from 0.1 through 1.0 to 10.0, α ranges from 0.81818 through 0 to -0.81818, and β ranges from 0.2338 through 0 to -0.2338 (i.e. $\beta = 0.2857\alpha$). Although tunneling is intrinsically a three-dimensional process, the remote stress for *steady-state tunneling* is estimated by an energy balance of the upstream uncracked state and the downstream cracked state. The downstream H-shape crack comprises a mode I crack of width $2a$ within material 1, and four delaminations each of length l, as depicted in Figure 3b.

During steady-state tunneling the tunneling front has a constant shape, and the energy release rate is independent of the tunneling length (and of the geometry of the initial flaw from which the tunneling crack initiated). Then, the energy released per unit tunneling depth can be computed as the difference in elastic strain energy ΔW upstream and downstream of the tunneling front (Hutchinson and Suo, 1992; Beuth, 1992; Ho and Suo, 1993). This energy drop equals the difference in strain energy for an uncracked plane-strain solid and for a cracked plane-strain solid. For the H-shape crack of Figure 3b the energy drop equals

$$\Delta W = \frac{1}{2}\sigma_{\text{inf},1}\overline{\delta}2a, \tag{8}$$

where $\sigma_{\text{inf},1}(= \bar{E}_1\varepsilon_{\text{inf}})$ equals the remote tensile stress in material 1 and $\overline{\delta}$ equals the average displacement over the mode I crack faces, according to

$$\overline{\delta} = \frac{1}{2a}\int_{-a}^{a} \delta(x)\,\mathrm{d}x. \tag{9}$$

By dimensional considerations, the average displacement $\overline{\delta}$ may be written in the form

$$\overline{\delta} = \frac{a\sigma_{\text{inf},1}}{\bar{E}_1} f\left(\frac{l}{a}, \frac{\bar{E}_2}{\bar{E}_1}\right), \tag{10}$$

where the dimensionless function f depends upon the aspect ratio of the H-shape crack l/a and the stiffness ratio $\bar{E}_2/\bar{E}_1$. Upon inserting Equation (10) into Equation (8), the energy drop per unit crack depth is

$$\Delta W = \frac{\sigma_{\text{inf},1}^2}{\bar{E}_1} a^2 f\left(\frac{l}{a}, \frac{\bar{E}_2}{\bar{E}_1}\right), \tag{11}$$

This energy drop can be related to the energy release rate for an H-shape tunneling crack G_{tun}, and to the energy release rate for plane-strain delamination G_d for each of the four delaminations of an H-shape crack, as follows.

3.1. Steady-state tunneling by an H-shape crack

The average energy release rate for unit advance of a tunneling H-shape crack, G_{tun}, is directly related to the energy drop ΔW by (Hutchinson and Suo, 1992; Beuth, 1992; Ho and Suo, 1993)

$$(2a + 4l)G_{\text{tun}} = \Delta W. \tag{12}$$

Also, the energy drop ΔW equals the energy required to form a mode I crack of length $2a$ in the central material 1 and four delaminations, each of length l . Upon designating the mode I toughness of material 1 as G_{Ic}, and the delamination toughness at the appropriate mode-mix as $G_{dc}(\psi(\hat{l}))$, the energy balance reads

$$\Delta W = (2a + 4l)G_{\text{tun}} = 2a\, G_{Ic} + 4l\, G_{dc}. \tag{13}$$

The remote stress for steady-state tunneling, $\sigma_{\text{tun}} = \sigma_{\text{inf},1}$, follows from Equations (13) and (11) as

$$\sigma_{\text{tun}} = \sqrt{\frac{\bar{E}_1(2a\, G_{Ic} + 4l\, G_{dc})}{a^2\, f(l/a, \bar{E}_2/\bar{E}_1)}}. \tag{14}$$

3.2. Plane-strain delamination

For the H-shape crack of Figure 3b the plane-strain energy release rate per unit advance of each delamination is

$$G_d = \frac{1}{4}\frac{\partial \Delta W}{\partial l}, \tag{15}$$

where the factor 4 reflects the number of delamination tips of the H-shape crack. Insertion of Equation (11) into Equation (15) yields

$$G_d = \frac{\sigma_{\text{inf},1}^2}{4\bar{E}_1} a f'\left(\frac{l}{a}, \frac{\bar{E}_2}{\bar{E}_1}\right), \tag{16}$$

where f' represents the partial derivative $f' = \partial f/\partial l$. The remote stress for plane-strain delamination, $\sigma_d = \sigma_{\text{inf},1}$ is obtained by substituting Equation (16) into Equation (7), and rearranging the expression to the form

$$\sigma_d = \sqrt{\frac{4\bar{E}_1\, G_{dc}}{a\, f'(l/a, \bar{E}_2/\bar{E}_1)}}. \tag{17}$$

4. Cracking in a 5/4 lay-up

Plane-strain delamination and steady-state tunneling are addressed for two different geometries, namely the 2/1 lay-up and the 5/4 lay-up. The notation '$n/(n-1)$ lay-up' refers to a laminate of n layers of material 1 alternately stacked with $n-1$ layers of material 2. Each layer of material 1 is of thickness $2a$ while the layers of material 2 have a thickness of $5a/3$. This thickness ratio is typical of that used for the fibre-metal laminates GLARE and ARALL, where aluminium sheets of thickness 0.2 to 0.4 mm are bonded by somewhat thinner fibre/epoxy layers (Marissen, 1988; Vermeeren, 1995; Takamatsu et al., 2001). Two cracked configurations of the 5/4 lay-up are investigated: an internal H-shape crack in the centre layer of the laminate, see Figure 4a, and a doubly deflected crack in the two outer layers of the laminate, see Figure 4b. The doubly deflected cracks in the two outer layers taken together

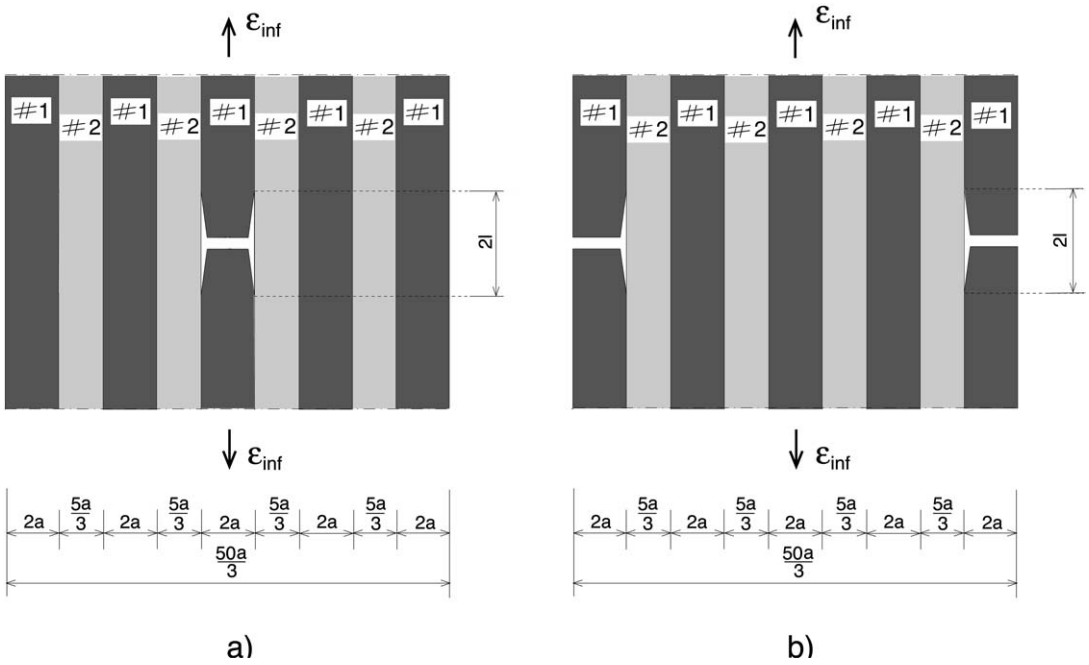

Figure 4. Cracking in a 5/4 lay-up. (a) H-shape crack in the centre layer of the laminate. (b) Doubly deflected crack in the two outer layers of the laminate.

resemble an H-shape crack of width $4a$. The results for the 5/4 lay-up are given first, and the results for the 2/1 lay-up are presented in a subsequent section.

4.1. Modelling aspects

The configurations in Figure 4 have been modelled with the aid of the finite element program ABAQUS Standard[1] . The degree of symmetry is such that only one quadrant is meshed. Fixed and roller supports impose the required symmetry and prevent rigid body motion. The strip is taken to be sufficiently long for end effects to be negligible: the top and bottom faces of the 5/4 lay-up are at a distance $200\,a$ from the delamination tip. H-shape cracks with delamination lengths in the range $0.015 < l/a < 40$ have been considered, using 7 different element meshes. Mesh refinement studies have been performed to check the convergence of the solution. All finite element configurations comprise 16 000 to 20 000 plane-strain 8-node iso-parametric elements, with 3×3 Gauss quadrature. At the delamination tip, the square root singularity of the stress field is simulated by moving the mid-side nodes on the crack flanks to the 1/4 point nearest to the crack tip. Additionally, for each crack tip element, three neighbouring nodes are collapsed to the crack tip.

A calculation of the load for steady-state tunneling and for plane-strain delamination of an H-shape crack requires the computation of:
(i) the displacements of the nodes situated on the mode I crack faces,
(ii) the path-independent J-integral at the delamination tip, as defined by (Rice, 1968)[2]

[1] Hibbitt, Karlsson & Sorensen, Inc., Pawtucket, RI, U.S.A.

[2] The J-integral, Equation (18), is path-independent when the crack is straight, traction free, with the material interface parallel to the crack.

$$J = \int_S \left[W n_1 - \sigma_{ij} n_i \frac{\partial u_j}{\partial x_1} \right] \mathrm{d}s, \tag{18}$$

(iii) the complex stress intensity factor at the delamination tip, $K = K_1 + i\, K_2$.

In Equation (18), S is any path that begins at the bottom crack face and ends at the top crack face, W is the elastic strain energy, n_i is the unit outward normal to the path S, σ_{ij} is the stress and u_i is the displacement. For a linear elastic material, the J-integral equals the energy release rate per unit crack advance, $G_d = J$, (Rice, 1968). The J-integral is computed as an embedded routine within ABAQUS by means of an area integral method that uses the virtual crack extension technique (Parks, 1974; Li et al., 1985). For each of the finite element models considered in the present study, the J-integral has been computed for 18 different annular rings around the crack tip: with the exception of the first annulus around the crack tip the computed integrals are in very good agreement (i.e. a scatter of less than 1% in value).

The J-integral provides the energy release rate for plane-strain delamination, $G_d = J$, and thereby the derivative f' via Equation (16). The remote stress for plane-strain delamination follows immediately from Equation (17). The complex stress intensity factor $K = K_1 + i\, K_2$ is required for determining the mode-mix $\psi(\hat{l})$, as defined by Equation (5). ABAQUS computes the real and imaginary components of the stress intensity factor, K_1 and K_2, by means of an interaction integral method. In this method, the components K_1 and K_2 are extracted from the energy release rate, Equation (6), by combining the solution of the actual crack tip field with that of an auxiliary field (Matos et al., 1989).

The computation of the displacements of the mode I crack faces gives the average crack opening displacement, Equation (9), and thereby the drop in strain energy, Equation (8) and its non-dimensional form f via Equation (11). As a next step, the energy release rate for tunneling, G_{tun} is computed from Equation (12), and the tunneling stress by means of Equation (14).

4.2. H-SHAPE CRACK IN CENTRE LAYER OF LAMINATE

4.2.1. *Mode-mix and energy release rate*

For the configuration in Figure 4a, the mode-mix $\psi = \text{atan}(\text{Im}(K\, a^{i\varepsilon})/\text{Re}(K\, a^{i\varepsilon}))$ has been computed as a function of the delamination length, l/a, and the results are presented in Figure 5a for selected values of stiffness mismatch, $\bar{E}_2/\bar{E}_1$, in the range 0.1 to 10.0. It is seen that the mode-mix at short crack lengths decreases from 72° to 50° with increasing stiffness ratio. For all stiffness ratios considered the mode-mix increases to 90° with increasing l/a. Accordingly, the delamination tip closes ($\text{Re}(K a^{i\varepsilon}) = 0$) and becomes a *pure mode II crack*. Because the influence of mode I contact has been neglected in the analysis (i.e. crack face overlap is allowed to occur), the current analysis is, strictly speaking, not applicable when delamination is in pure mode II. However, Dollar and Steif (1991a) have demonstrated that for an H-shape crack in a homogeneous, infinite medium, the mode II stress intensity factor for a frictionless crack with and without crack face overlap only show minor differences. In other studies of mixed mode delamination this feature was assumed to hold on the basis of heuristic reasoning (Liechti and Chai, 1992; Hutchinson and Lu, 1995; Lu, 1996). Thus, it is expected that the computed energy release rates are not greatly in error when the effect of crack surface contact is neglected.

Figure 5b depicts the energy release rate for plane-strain delamination G_d versus delamination length, l/a. Note that a *zero offset* in the scale for l/a has been used in order to clarify the asymptotic behaviour as $l/a \to 0$. At short delamination lengths, $l/a < 1$, the energy release rate is sensitive to l. For the asymptotic case $l/a \to 0$, the energy release rate tends

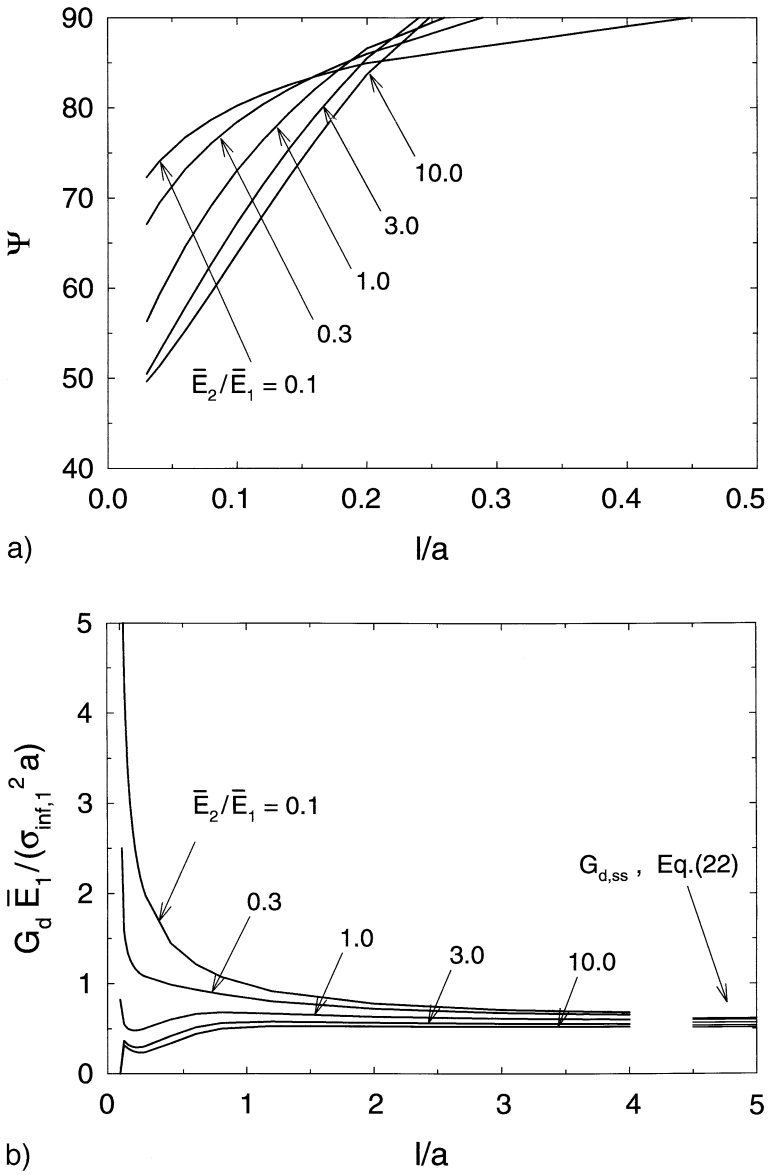

Figure 5. Cracking in the centre layer of the 5/4 lay-up, see Figure 4a. (a) Mode-mixity, $\psi = \text{atan}(\text{Im}(K\, a^{i\epsilon})/\text{Re}(K\, a^{i\epsilon}))$, versus delamination length l/a. (b) Energy release rate for plane-strain delamination G_d versus delamination length l/a.

to zero when $\bar{E}_2/\bar{E}_1 > 1$ and becomes unbounded when $\bar{E}_2/\bar{E}_1 < 1$, as discussed by He and Hutchinson (1989), Ye et al. (1992), and Lu (1996). For a homogeneous laminate, $\bar{E}_2/\bar{E}_1 = 1$, the plane-strain energy release rate remains finite when $l/a \to 0$, and the $\psi(l/a)$ and $G_d(l/a)$ curves are in good agreement with those obtained by Lu (1996) for an H-shape crack in an infinite medium.

When $l/a > 1$, the energy release rate slowly asymptotes to a steady-state value with increasing l. The depicted steady-state values, $G_{d,ss} = G_d(l/a \to \infty)$, can be derived analytically by calculating the difference in the elastic strain energy downstream and upstream of

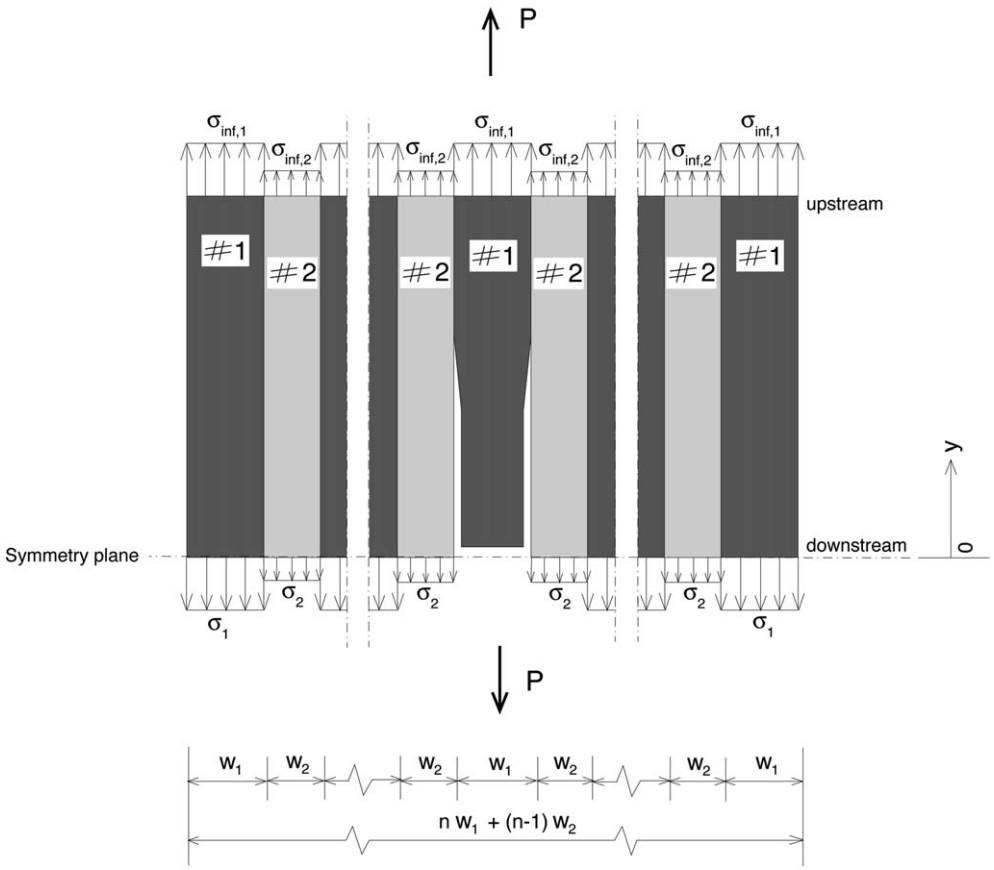

Figure 6. H-shape crack in a laminate consisting of n layers of material 1 and $n-1$ layers of material 2. The force P denotes the equilibrium between the 'upstream' and 'downstream' cross-sections.

the delamination tip. Consider a laminate consisting of n layers of material 1 with width w_1, and $n-1$ layers of material 2 with width w_2, as sketched in Figure 6. The axial force per unit thickness, P, is related to the remote stress in layer 1, $\sigma_{\text{inf},1} = \bar{E}_1 \varepsilon_{\text{inf}}$, and to the remote stress in layer 2, $\sigma_{\text{inf},2} = \bar{E}_2 \varepsilon_{\text{inf}}$, by

$$P = n\,\sigma_{\text{inf},1} w_1 + (n-1)\sigma_{\text{inf},2} w_2. \tag{19}$$

Additionally, on the symmetry plane $y = 0$, the axial force is

$$P = (n-1)\sigma_1 w_1 + (n-1)\sigma_2 w_2, \tag{20}$$

where σ_1 and σ_2 are the (uniform) stresses at $y = 0$ in materials 1 and 2, respectively. Equating Equations (19) and (20) and using the compatibility statement $\sigma_1/\bar{E}_1 = \sigma_2/\bar{E}_2$ it follows that

$$\begin{aligned} \sigma_1 &= \gamma\,\sigma_{\text{inf},1} \\ \sigma_2 &= \frac{\bar{E}_2}{\bar{E}_1}\gamma\,\sigma_{\text{inf},1} \end{aligned} \qquad \text{where} \quad \gamma \equiv \frac{n\bar{E}_1 w_1 + (n-1)\bar{E}_2 w_2}{(n-1)(\bar{E}_1 w_1 + \bar{E}_2 w_2)}. \tag{21}$$

The steady-state energy release rate at an individual delamination tip, $G_{d,ss}$, is calculated from the energy difference upstream and downstream of the delamination tip (Hutchinson and Suo, 1992). Employing Equation (21), this yields

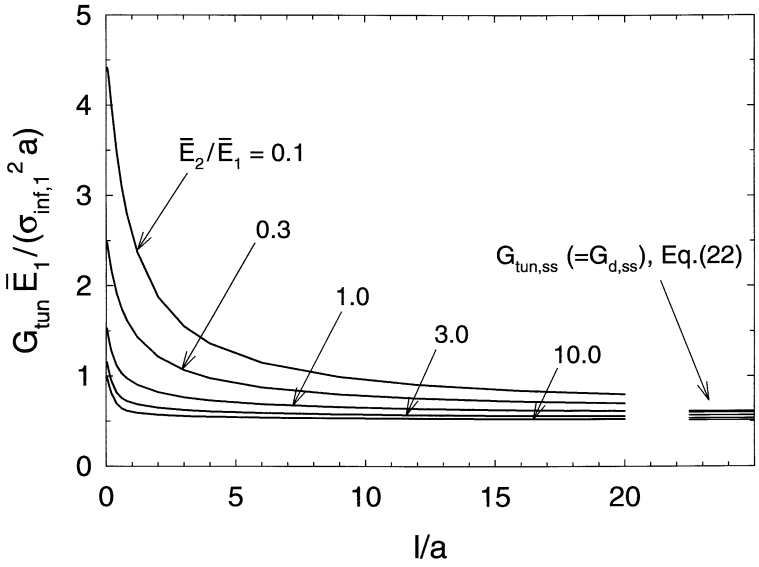

Figure 7. Energy release rate for steady-state tunneling G_{tun} versus delamination length l/a (cracking in the centre layer of the 5/4 lay-up, see Figure 4a).

$$G_{d,ss} = \frac{\sigma_{\text{inf},1}^2}{4\,\bar{E}_1}\left(w_1\gamma^2(n-1) + \frac{\bar{E}_2}{\bar{E}_1}w_2\gamma^2(n-1) - w_1 n - \frac{\bar{E}_2}{\bar{E}_1}w_2(n-1)\right). \tag{22}$$

Note that the structure of the above expression obeys the general expression, Equation (16). The steady-state energy release rates plotted in Figure 5b correspond to Equation (22), where $n = 5$, $w_1 = 2a$ and $w_2 = 5a/3$. It is clear from Figure 5b that the finite element predictions lay close to the analytical asymptotes when $l/a > 2$ (Additional checks reveal that at $l/a = 40$, all curves have approached their steady-state value to within 0.4%.).

Figure 7 displays the energy release rate for tunneling, G_{tun}, as a function of the relative delamination length, l/a. At short delamination lengths, $l/a < 3$, the energy release rate drops rapidly with increasing delamination length for all stiffness mismatches considered. In comparison with the energy release rate for plane-strain delamination (Figure 5b), greater delamination lengths are required to attain a steady-state. For example, for the stiffness ratios $\bar{E}_2/\bar{E}_1 = 0.1$ and 10.0, the energy release rate for tunneling at $l/a = 40$ are 15% higher and 1% higher, respectively, than the steady-state values Equation (22). The fact that a higher stiffness ratio induces a faster convergence towards a steady state is also evident from Figure 7.

It is noteworthy that the steady-state values depicted in Figures 5b and 7 are identical, i.e. $G_{\text{tun},ss} = G_{d,ss}$. This can be explained as follows. As argued by Beuth (1992), the condition $G_{\text{tun}} = G_d$ is generally fulfilled at any point on the G_{tun} versus l/a curve where $\partial G_{\text{tun}}/\partial l = 0$. In the present problem, $\partial G_{\text{tun}}/\partial l \to 0$ as $l/a \to \infty$, and so $G_{\text{tun},ss} = G_{d,ss}$.

4.2.2. *Failure mechanisms*

It is instructive to plot the tunneling stress, σ_{tun}, and the stress for plane-strain delamination, σ_d, as functions of l/a for the cases $\bar{E}_2/\bar{E}_1 = 0.1$, 1.0 and 10.0, see Figures 8a, 8b and 8c, respectively. The tunneling stress is evaluated using Equation (14), and selected values for the toughness ratio G_{dc}/G_{Ic}. The stress for plane-strain delamination follows from Equation (17). It has been noted above that the plane-strain delamination is purely mode II, except for short delamination lengths, and so it can be assumed that G_{dc} is constant in the calculation of σ_{tun}.

The $\sigma_d(l/a)$ curve may be interpreted as the crack growth resistance curve (or R-curve) for plane-strain delamination. The depicted steady-state stress, $\sigma_{ss} = \sigma_d(l/a \to \infty) = \sigma_{\text{tun}}(l/a \to \infty)$, is derived by substituting Equation (7) into Equation (22), giving

$$\sigma_{ss} = \sqrt{\frac{4\,\bar{E}_1 G_{dc}}{w_1(\gamma^2(n-1)-n) + \dfrac{\bar{E}_2}{\bar{E}_1} w_2(\gamma^2-1)(n-1)}}, \tag{23}$$

where the dimensionless parameter γ is defined in Equation (21). The normalisation chosen for $\sigma_{\text{tun}}(l/a)$ and $\sigma_d(l/a)$ in Figures 8a–c involves G_{dc} rather than G_{Ic}. Consequently, curves of increasing ratio G_{dc}/G_{Ic} should be interpreted as curves of diminishing mode I toughness G_{Ic} for the mid-layer (material 1). Further, three different fracture scenarios can be distinguished in Figures 8a–c, which depend upon the toughness ratio G_{dc}/G_{Ic} and upon the elastic mismatch ratio $\bar{E}_2/\bar{E}_1$. Each scenario has already been sketched in Figure 2, and is discussed below with reference to the current 5/4 lay-up.

First, consider the tunneling stress $\sigma_{\text{tun}}(l/a)$ and the plane-strain delamination stress $\sigma_d(l/a)$ for the choice $\bar{E}_2/\bar{E}_1 = 0.1$, see Figure 8a. Again, a zero offset in the scale for l/a has been used in order to clarify the asymptotic behaviour as $l/a \to 0$. Stable plane-strain delamination is characterised by a rising $\sigma_d(l/a)$ response. Correspondingly, stable tunneling of an H-shape crack occurs for $G_{dc}/G_{Ic} \geq 0.08$, with the *minimum* tunneling stress $\sigma_{\text{inf},1} = \sigma_{\text{tun,min}}$ indicated by the intersection points (black dots) between the $\sigma_d(l/a)$ curve and the $\sigma_{\text{tun}}(l/a)$ curve for each selected value of G_{dc}/G_{Ic}. The value of l/a at the minimum tunneling stress $\sigma_{\text{tun,min}}$ reflects the (*constant*) delamination length of the tunneling H-shape crack, $l/a = (l/a)_{\text{tun}}$. In Figure 2 this fracture scenario has been designated as *mechanism 2*. The fact that the intersection points correspond to an extremum (*minimum*) for the tunneling stress can be made evident by applying the condition $\partial\sigma_{\text{tun}}/\partial l = 0$ to Equation (14), yielding $\sigma_{\text{tun}} = \sigma_d$, where σ_d is given by Equation (17). A similar conclusion has been drawn by Cox and Marshall (1996) for the tunneling of a mode I transverse ply crack in a laminated ceramic composite, and by Fleck and Zhao (2000) for the microbuckle tunneling in a fibre-reinforced laminate. The delamination length for this mechanism is stable, since at the minimum tunneling stress the tangent of the $\sigma_d(l/a)$ curve is positive (R-curve behaviour). In contrast, for $G_{dc}/G_{Ic} < 0.08$, the $\sigma_{\text{tun}}(l/a)$ curve decreases monotonically with increasing l/a and correspondingly the minimum tunneling stress becomes $\sigma_{\text{tun,min}} = \sigma_{\text{tun}}(l/a \to \infty) = \sigma_{ss}$. As a consequence, unstable delamination will occur in all directions. In Figure 2 this fracture scenario has been designated as *mechanism 3*.

Second, consider the tunneling stress $\sigma_{\text{tun}}(l/a)$ and the plane-strain delamination stress $\sigma_d(l/a)$ for the choice $\bar{E}_2/\bar{E}_1 = 1.0$, see Figure 8b. It is noted that $\sigma_d(l/a)$ has a single oscillation in value for $0 < l/a < 1$; this feature is not a numerical artefact. The $\sigma_d(l/a)$ curve has two rising portions, one at $0 < l/a < 0.12$ and one for $l/a > 0.80$. Although the latter rising portion has a small slope, nonetheless it gives rise to the existence of *mechanism 2*, for reasons explained above. For a relatively high toughness ratio $G_{dc}/G_{Ic} \geq 0.52$ the $\sigma_{\text{tun}}(l/a)$ curve lays below the $\sigma_d(l/a)$ curve with no intersection points between the two curves. The minimum tunneling stress $\sigma_{\text{tun,min}}$ is achieved at $l/a = 0$, implying tunneling of a mode I crack within the mid-layer and delamination absent. This fracture scenario has been designated in Figure 2 as *mechanism 1*. For moderate toughness ratios, $0.28 < G_{dc}/G_{Ic} < 0.52$, stable tunneling occurs with a constant delamination length (*mechanism 2*), and for low toughness ratios, $G_{dc}/G_{Ic} \leq 0.28$, unstable delamination operates in all directions (*mechanism 3*).

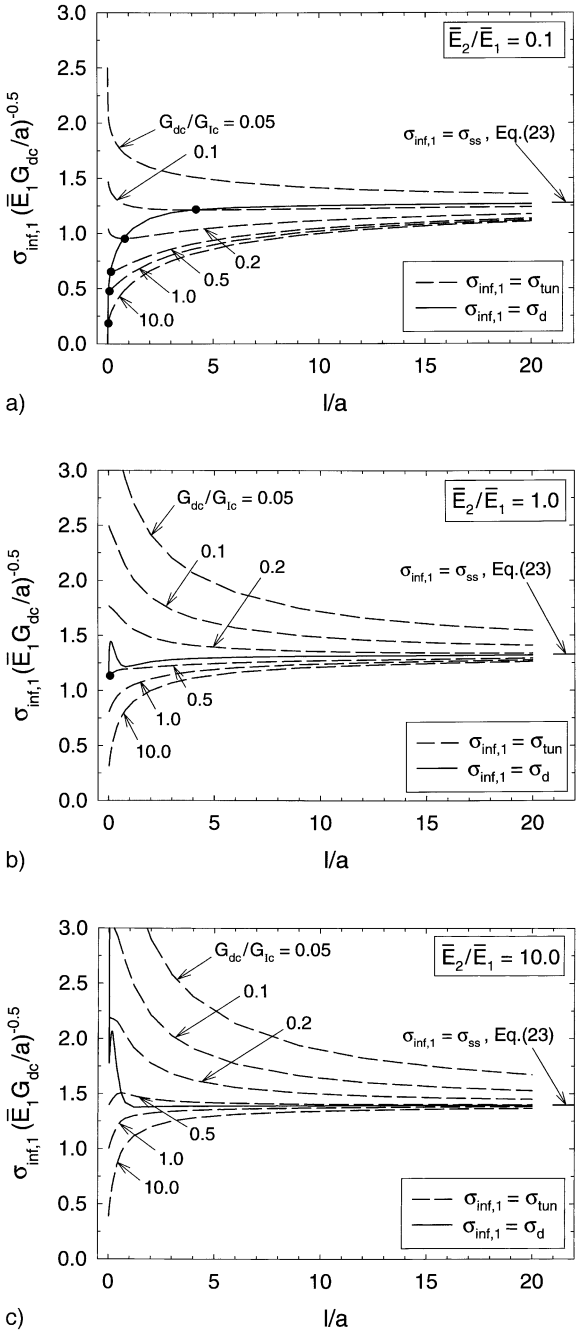

Figure 8. Remote stress $\sigma_{\text{inf},1}$ versus delamination length l/a (cracking in the centre layer of the 5/4 lay-up, see Figure 4a). Solid line designates the plane-strain delamination curve $\sigma_d - l/a$ and dashed lines designate the (steady-state) tunneling curves $\sigma_{\text{tun}} - l/a$ for selected toughness ratios G_{dc}/G_{Ic}. The black dots indicate the minimum tunneling stress for *mechanism 2*. (a) $\bar{E}_2/\bar{E}_1 = 0.1$. (b) $\bar{E}_2/\bar{E}_1 = 1.0$. (c) $\bar{E}_2/\bar{E}_1 = 10.0$.

Third, $\sigma_{\text{tun}}(l/a)$ and $\sigma_d(l/a)$ are plotted in Figure 8c for the choice $\bar{E}_2/\bar{E}_1 = 10.0$. The delamination stress σ_d shows a minimum at $l/a = 1$; it rises slightly in value as l/a increases to infinity, but rises steeply as l/a drops to zero (A minor oscillation in $\sigma_d(l/a)$ is noted at $l/a = 0.03$, but this local perturbation in value is considered no further). The shape of the plane strain delamination curve $\sigma_d(l/a)$ is consistent with the following crack tunneling behaviour $\sigma_{\text{tun}}(l/a)$. For $G_{dc}/G_{Ic} \geq 0.62$, the $\sigma_{\text{tun}}(l/a)$ curve is monotonically rising and this implies that *mechanism 1* with $l/a = 0$ operates[3]. For $0.58 < G_{dc}/G_{Ic} < 0.62$, a local minimum in $\sigma_{\text{tun}}(l/a)$ is demanded from the rising part of the $\sigma_d(l/a)$ curve and *mechanism 2* is predicted. Finally, for $G_{dc}/G_{Ic} \leq 0.58$, the tunneling stress $\sigma_{\text{tun}}(l/a)$ has an unstable maximum value at the intersection with the $\sigma_d(l/a)$ curve, and drops monotonically at larger l/a: *mechanism 3* is active, and $\sigma_{\text{tun,min}} = \sigma_{ss}$ at $l/a \to \infty$.

4.2.3. *Analytical estimate for the tunneling stress by mechanism 1*

For a homogeneous laminate ($\bar{E}_1 = \bar{E}_2$), the tunneling stress by *mechanism 1* can be determined from the classical solution to the corresponding plane-strain crack problem. Consider a mode I crack of length $2a'$ in a plate of width w loaded under a uniaxial tensile stress σ_{inf}; then, the stress intensity factor K_I at the crack tip is (Broek, 1986)

$$K_I = \sigma_{\text{inf}}\sqrt{\pi a'}\, g(a'/w), \tag{24}$$

with g a dimensionless function that depends upon the non-dimensional crack length a'/w. The plane-strain energy release rate at the mode I crack tip follows from Equation (24) as

$$G_I = \frac{K_I^2}{\bar{E}_1} = \frac{\sigma_{\text{inf}}^2 \pi a'}{\bar{E}_1} g^2(a'/w). \tag{25}$$

Now, Dvorak and Laws (1986) have demonstrated that the energy release rate at a crack tip of a tunneling mode I crack with width $2a$ can be calculated by means of the integral relation

$$G_{\text{tun}} = \frac{1}{a}\int_0^a G_I(a')\,\mathrm{d}a'. \tag{26}$$

For the geometry shown in Figure 4a, the ratio of crack length to specimen width is sufficiently small ($a/w = 3/50$) for the approximation $g(a/w) \approx 1$ to be justified. Substituting Equation (25) into (26) then gives

$$G_{\text{tun}} = \frac{\pi \sigma_{\text{inf}}^2\, a}{2\,\bar{E}_1}. \tag{27}$$

Upon equating the energy release rate for tunneling to the mode I toughness, $G_{\text{tun}} = G_{Ic}$, the critical stress for steady-state tunneling of the mode I crack directly follows from Equation (27) as

$$\sigma_{\text{tun}} = \sqrt{\frac{2\,\bar{E}_1\, G_{Ic}}{\pi a}} \tag{28}$$

Similar derivations can be found in Beuth (1992) and Ho and Suo (1993). For the homogeneous case depicted in Figure 8b, a numerical check on the tunneling stress for *mechanism 1*,

[3]Since $\bar{E}_2/\bar{E}_1 > 1$, the crack stands off the interface by a small distance within the more compliant material 1, and the predicted tunneling stress is slightly below that given here (see Beuth, 1992).

$\sigma_{\text{tun}}(l/a = 0)$, can be made via Equation (28). Although not shown here, the numerical values agree within one percent of the analytical estimate, Equation (28), for each choice of G_{dc}/G_{Ic}.

As an additional check on the numerical results the asymptotic value for plane strain delamination, $\sigma_d(l/a \to 0)$, at $\bar{E}_2/\bar{E}_1 = 1$ can be obtained via Equation (25), and can be compared with the numerical prediction in Figure 8b. Using the results obtained by He et al. (1994), in an infinite homogeneous medium the ratio between the energy release rate for delamination and mode I cracking can be computed as $G_d/G_I = 0.261$ for a delamination length approaching to zero. Combining this result with Equation (25), it follows that $G_d(l/a \to 0) = 0.82\sigma_d^2 a/\bar{E}_1$. Hence, $\sigma_d(\bar{E}_1 G_{dc}/a)^{-0.5} = 1.104$ as $l/a \to 0$, which closely corresponds to the numerical prediction.

4.2.4. *Failure mechanism map*

A failure mechanism map can be constructed, in which the minimum tunneling stress $\sigma_{\text{tun,min}}$ is plotted against the toughness ratios G_{dc}/G_{Ic}, see Figure 9a. The figure can be used to estimate the (critical) tunneling stress for assumed values of G_{dc}/G_{Ic} and $\bar{E}_2/\bar{E}_1$. The three failure modes are displayed with the location of their boundaries indicated by dashed lines. Stable tunneling (*mechanism 2*) dominates the map for $\bar{E}_2/\bar{E}_1 < 1$. For each curve of tunneling stress versus toughness ratio the transition from one mechanism to another is indicated by a black dot. At low toughness ratios *mechanism 3* operates and the tunneling stress is given by Equation (23). At higher toughness ratios and for $\bar{E}_2/\bar{E}_1 \geq 1$ *mechanism 1* operates; alternatively, at higher toughness ratios and for $\bar{E}_2/\bar{E}_1 < 1$ *mechanism 2* operates.

The corresponding values of the delamination length at tunneling are shown in Figure 9b as a function of the toughness ratio G_{dc}/G_{Ic}. For $\bar{E}_2/\bar{E}_1 = 3.0$ and 10.0 it is difficult to obtain the precise shape of the curve in the transition from *mechanism 1* ($(l/a)_{\text{tun}} = 0$) to *mechanism 3* ($(l/a)_{\text{tun}} \to \infty$); this transition occurs abruptly due to the small range of G_{dc}/G_{Ic} values over which *mechanism 2* is operational, see Figure 9a. Hence, for $\bar{E}_2/\bar{E}_1 = 3.0$ and 10.0 the anticipated trends for *mechanism 2* are represented by dashed lines. It is concluded from Figure 9b that H-shape cracking with a finite delamination length, exceeding $(l/a)_{\text{tun}} = 0.1$, only occurs over a narrow range of values for G_{dc}/G_{Ic}.

For (relatively high) toughness ratios where $0 < (l/a)_{\text{tun}} < 0.1$, it becomes difficult experimentally to distinguish between *mechanism 2* with delamination present, and *mechanism 1* with delamination absent.

4.3. Deflected crack in two outer layers of laminate

4.3.1. *Mode-mix and energy release rate*

The configuration of a doubly deflected crack in each of the two outer layers of the 5/4 lay-up has been depicted in Figure 4b. The mode-mix at the delamination tip of the cracks is sketched in Figure 10a for various delamination lengths. For the stiffness ratios considered, a steady state is attained relatively quickly with increasing l/a, and the steady-state mode-mix generally lies between 50° and 60°. Recall that the steady-state mode-mix for the H-shape crack in the centre layer of the 5/4 lay-up (Figure 5a) equals 90° (i.e. pure mode II).

The energy release rate for plane-strain delamination is plotted against the delamination length l/a in Figure 10b. As in Figure 5b, the energy release rate rapidly attains a steady-state with increasing l/a. The steady-state energy release rate for the configuration in Figure 4b can be derived in a similar manner to that given in Section 4.2.1 for the configuration in Figure 4a, and the resulting closed-form expression is

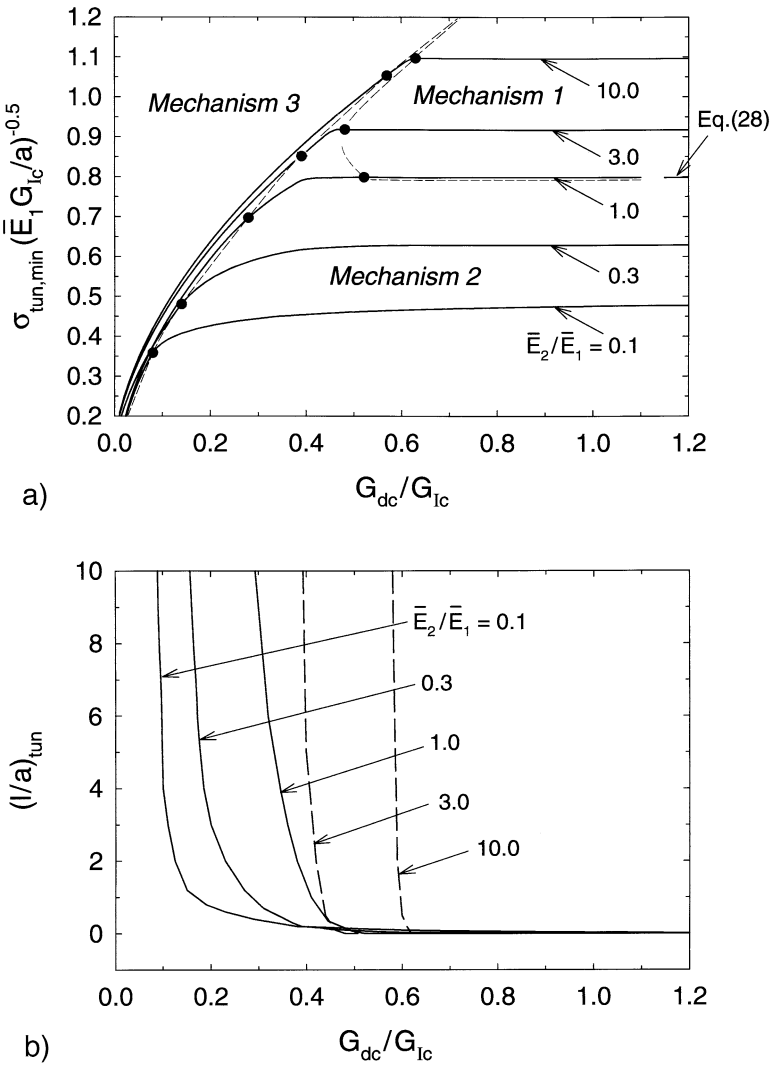

Figure 9. Cracking in the centre layer of the 5/4 lay-up, see Figure 4a. (a) Minimum tunneling stress $\sigma_{\text{tun,min}}$ versus fracture toughness ratio G_{dc}/G_{Ic}. Dashed lines indicate the zones corresponding to the three failure mechanisms in Figure 2. (b) Delamination length $(l/a)_{\text{tun}}$ versus fracture toughness ratio G_{dc}/G_{Ic}.

$$G_{d,ss} = \frac{\sigma_{\text{inf},1}^2}{4\,\bar{E}_1}\left(w_1\lambda^2(n-2) + \frac{\bar{E}_2}{\bar{E}_1}w_2\lambda^2(n-1) - w_1 n - \frac{\bar{E}_2}{\bar{E}_1}w_2(n-1)\right), \tag{29}$$

where

$$\lambda \equiv \frac{n\,\bar{E}_1 w_1 + (n-1)\bar{E}_2 w_2}{(n-2)\bar{E}_1 w_1 + (n-1)\bar{E}_2 w_2}.$$

4.3.2. *Failure mechanisms*

The $\sigma_d(l/a)$ and $\sigma_{\text{tun}}(l/a)$ curves are plotted in Figures 11a, b and c for the stiffness mismatches $\bar{E}_2/\bar{E}_1 = 0.1$, 1.0 and 10.0, respectively. A comparison with the failure curves for the H-shape crack in the centre layer of the 5/4 lay-up (Figure 8) reveals that the responses are

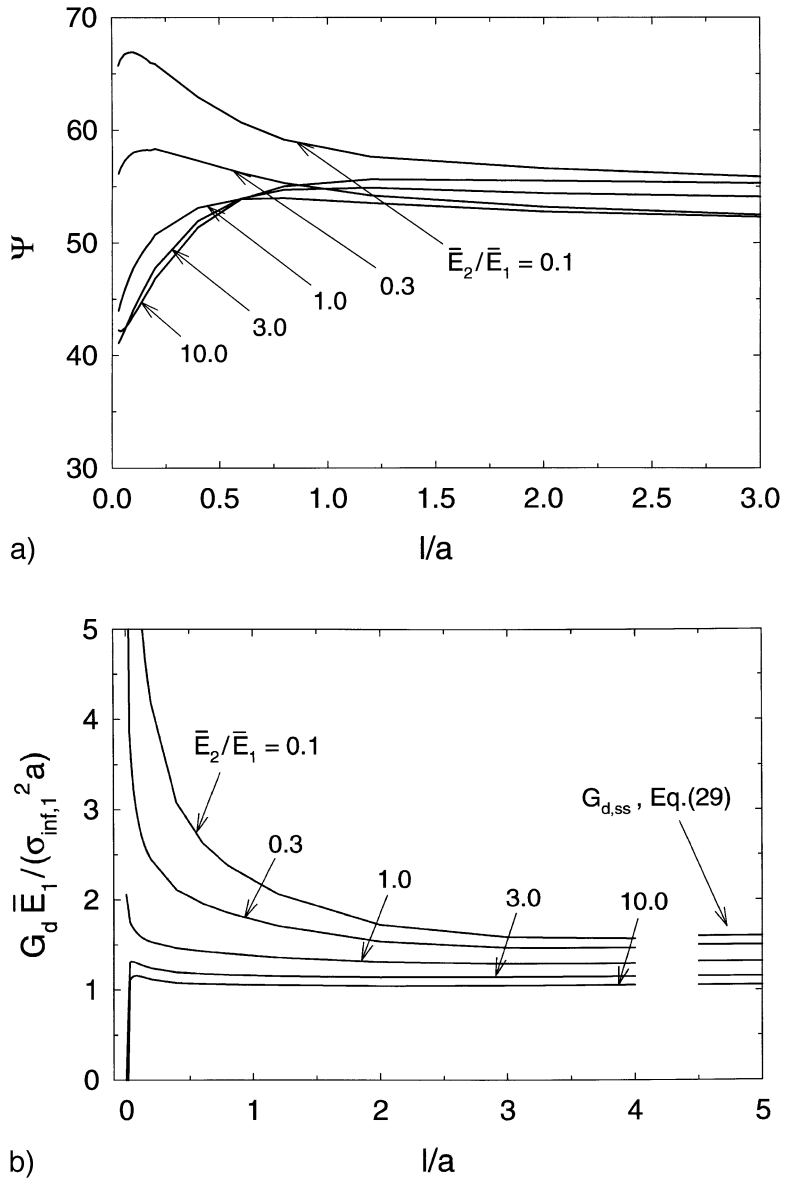

Figure 10. Cracking in the two outer layers of the 5/4 lay-up, see Figure 4b. (a) Mode-mixity, $\psi = \text{atan}(\text{Im}(K\,a^{i\epsilon})/\text{Re}(K\,a^{i\epsilon}))$, versus delamination length l/a. (b) Energy release rate for plane-strain delamination G_d versus delamination length l/a.

qualitatively similar. Thus, the discussion on the three failure mechanisms (see Section 4.2.2) also applies to the current case. The stress levels are a little lower than those for the H-shape crack in the centre layer of the 5/4 lay-up, due to the presence of the free surface. The steady-state stress, σ_{ss}, has been computed by combining Equations (7) and (29),

$$\sigma_{ss} = \sqrt{\frac{4\,\bar{E}_1 G_{dc}}{w_1(\lambda^2(n-2)-n) + \dfrac{\bar{E}_2}{\bar{E}_1} w_2(\lambda^2-1)(n-1)}} \tag{30}$$

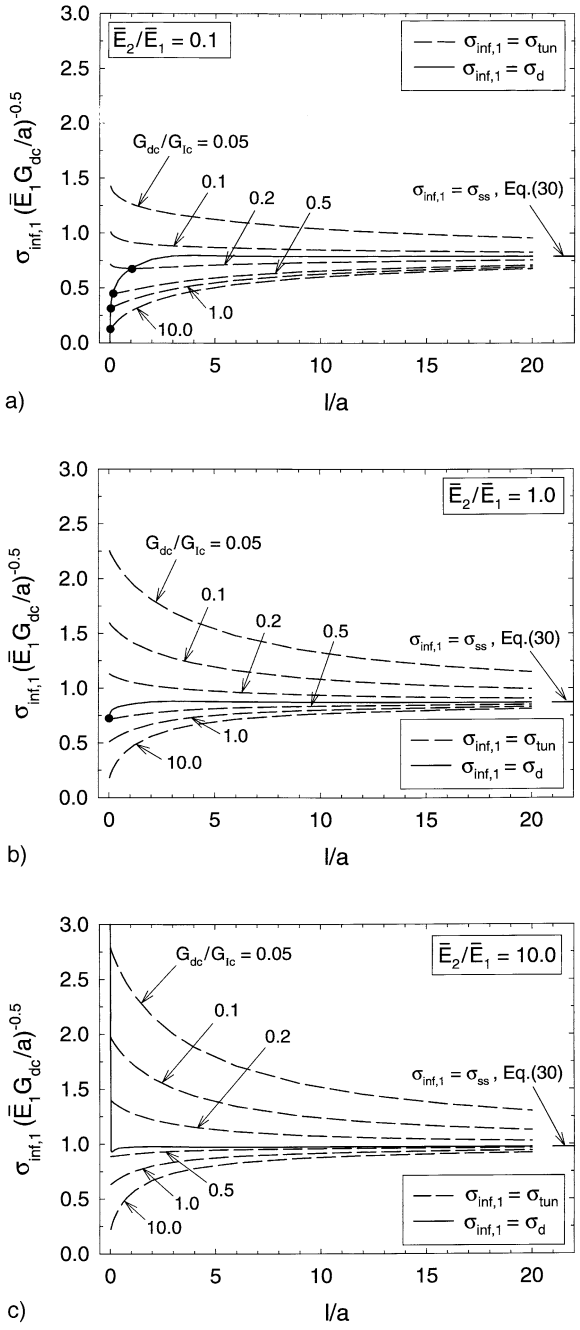

Figure 11. Remote stress $\sigma_{\text{inf},1}$ versus delamination length l/a (cracking in the two outer layers of the 5/4 lay-up, see Figure 4b). Solid line designates the plane-strain delamination curve $\sigma_d - l/a$ and dashed lines designate the (steady-state) tunneling curves $\sigma_{\text{tun}} - l/a$ for selected toughness ratios G_{dc}/G_{Ic}. The black dots indicate the minimum tunneling stress for mechanism 2. (a) $\bar{E}_2/\bar{E}_1 = 0.1$. (b) $\bar{E}_2/\bar{E}_1 = 1.0$. (c) $\bar{E}_2/\bar{E}_1 = 10.0$.

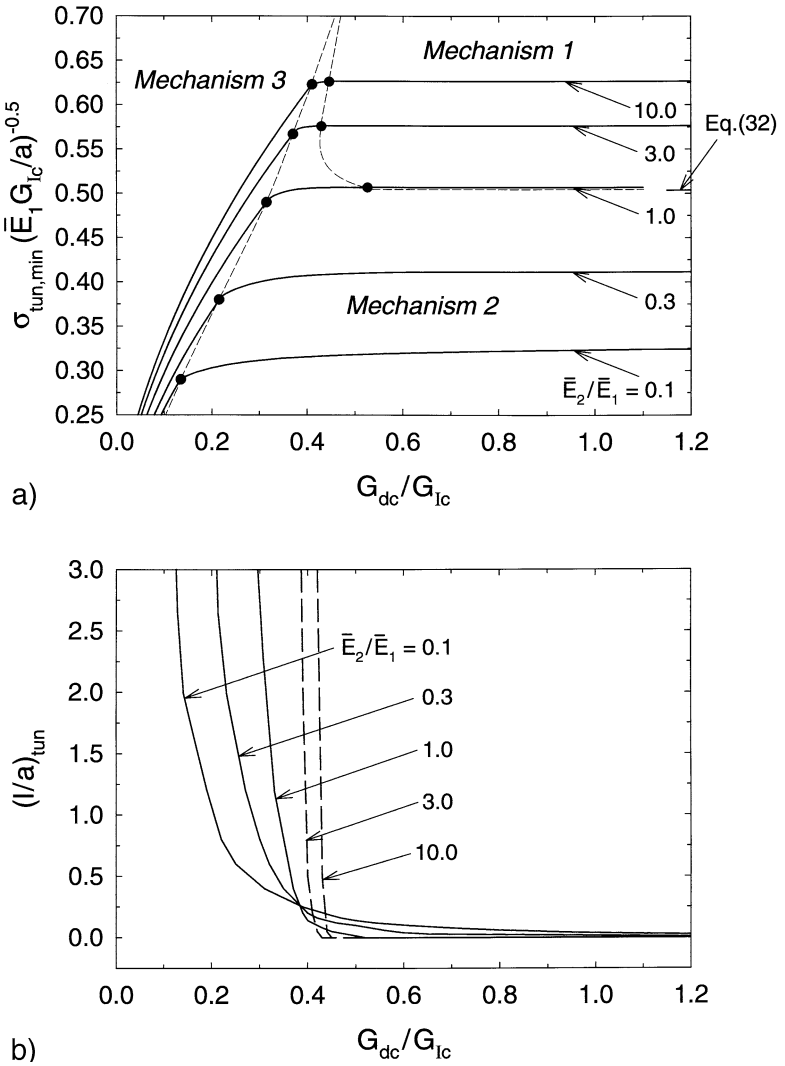

Figure 12. Cracking in the two outer layers of the 5/4 lay-up, see Figure 4b. (a) Minimum tunneling stress $\sigma_{\text{tun,min}}$ versus fracture toughness ratio G_{dc}/G_{Ic}. Dashed lines indicate the zones corresponding to the three failure mechanisms in Figure 2. (b) Delamination length $(l/a)_{\text{tun}}$ versus fracture toughness ratio G_{dc}/G_{Ic}.

Figures 11a–c illustrate that the above closed-form expression provides correct asymptotes for the numerical results.

The minimum tunneling stress $\sigma_{\text{tun,min}}$ is plotted against the toughness ratio G_{dc}/G_{Ic} in Figure 12a, with the failure mechanisms superimposed on the plot. The failure mechanism map for the doubly deflected cracks in the outer layers appears to be qualitatively similar to that shown in Figure 9a for the internal H-shape crack of the 5/4 laminate.

For a double mode I edge crack with individual crack lengths $2a'$ generated in a homogeneous laminate under a uniaxial tensile stress σ_{inf}, the stress intensity factor at the crack tip is (Broek, 1986)

$$K_I = 1.12\,\sigma_{\text{inf}}\sqrt{\pi 2a'}\,g(a'/w). \tag{31}$$

Using the procedure outlined via Equations (24) to (28), the tunneling stress is

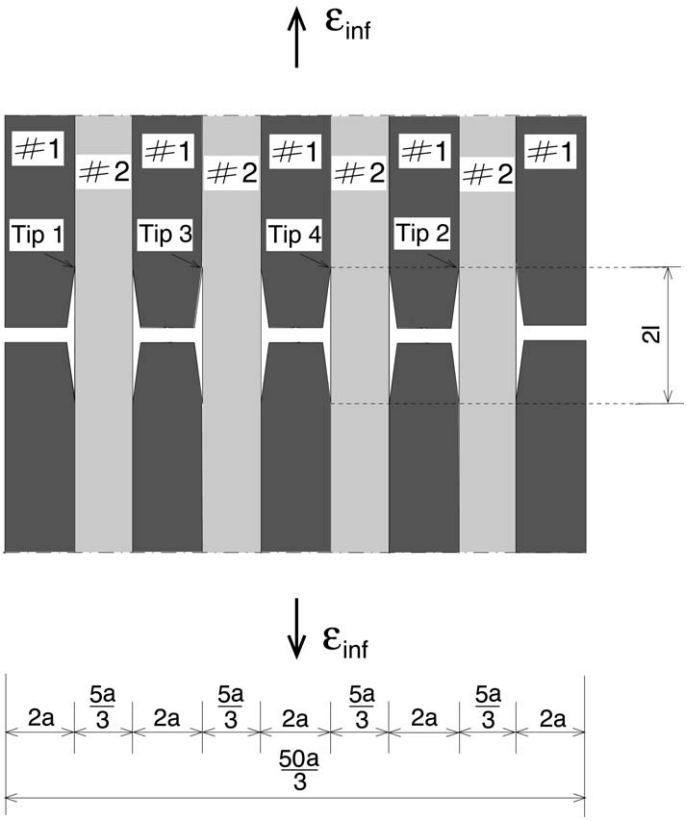

Figure 13. Uniform cracking in a 5/4 lay-up.

$$\sigma_{\text{tun}} = \frac{1}{1.12}\sqrt{\frac{\bar{E}_1 G_{Ic}}{\pi a}}. \tag{32}$$

Although this stress level corresponds to the asymptotic case where $a/w \to 0$, Figure 12a reveals that it closely approaches the critical stress for the homogeneous 5/4 lay-up. In Figure 12b the delamination lengths are sketched as a function of the toughness ratio G_{dc}/G_{Ic}. For $\bar{E}_2/\bar{E}_1 < 1$, *mechanism 2* is active over a wide range of toughness ratios G_{dc}/G_{Ic}, but for most of this range (i.e. $G_{dc}/G_{Ic} > 0.4$) the corresponding delamination $(l/a)_{tun}$ is almost zero. In contrast, for $\bar{E}_2/\bar{E}_1 \geq 1$, *mechanism 2* is active only over a narrow range of G_{dc}/G_{Ic}, see also Figure 12a.

4.4. Multiple delamination of the 5/4 lay-up

So far, delamination of a single mid-layer and of two outer layers have been addressed. In reality, stacked laminates have the possibility of delaminating at several interfaces. In order to assess this, plane-strain delamination of all interfaces is addressed for a 5/4 lay-up, with each delamination of length $l/a = 2$, see Figure 13. The choice $l/a = 2$ was made in order to obtain values of the mode-mix ψ and the plane strain energy release rate G_d near steady-state. The representative delamination tips are labelled 1 to 4, with a higher number indicating that the tip is located further from the free edge. The mode-mix and the plane strain energy release rate for the four delamination tips have been calculated as a function of the stiffness

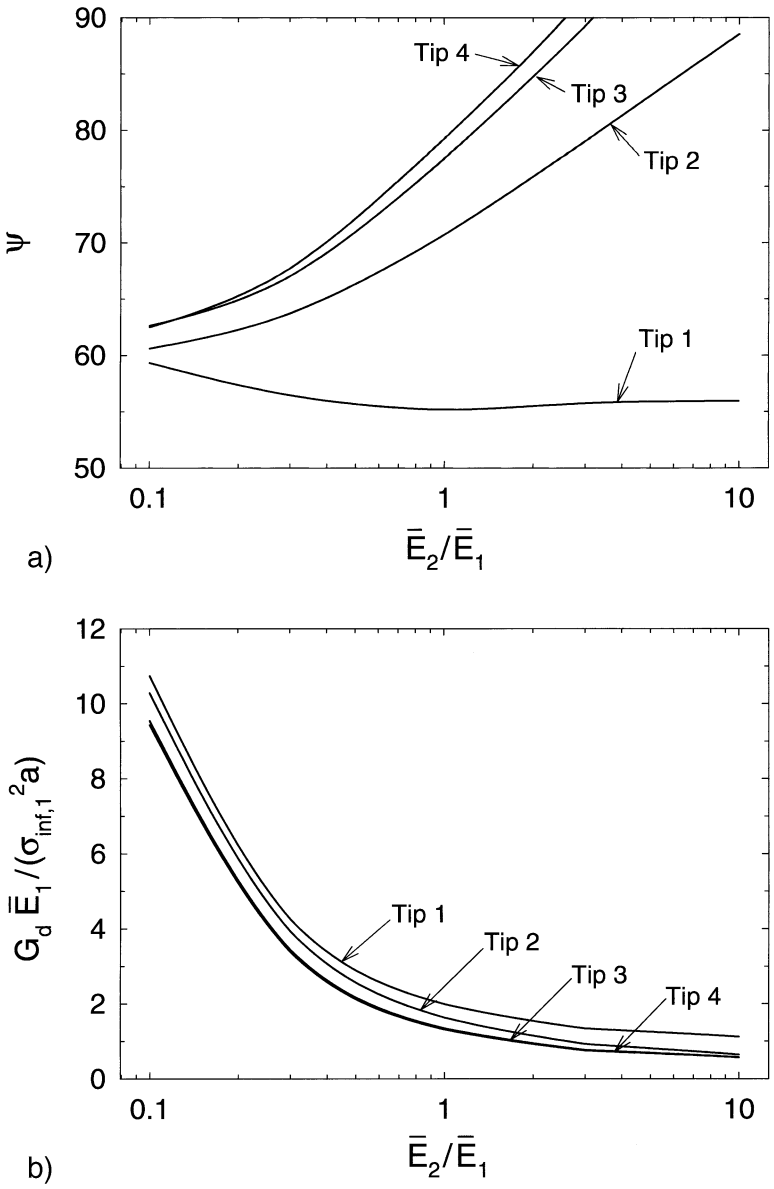

Figure 14. Uniform cracking in a 5/4 lay-up, see Figure 13. (a) Mode-mixity, $\psi = \text{atan}(\text{Im}(K\,a^{i\epsilon})/\text{Re}(K\,a^{i\epsilon}))$, versus delamination length l/a. (b) Energy release rate for plane-strain delamination G_d versus delamination length l/a.

mismatch $\bar{E}_2/\bar{E}_1$, and the results are plotted in Figures 14a and b, respectively. For tips 2, 3 and 4 the mode-mix ψ increases to the mode II limit ($\psi = 90°$) with increasing $\bar{E}_2/\bar{E}_1$; for tip 1, however, ψ remains approximately constant at 57° – 60°. Evaluations have also been made of the interfacial stress intensity factor $K\,a^{i\varepsilon}$, but the plots are omitted for the sake of brevity. The mode I stress intensity factor, $\text{Re}(K\,a^{i\varepsilon})$, drops to zero with increasing $\bar{E}_2/\bar{E}_1$ for tips 2, 3 and 4, but is relatively insensitive to the value of $\bar{E}_2/\bar{E}_1$ for tip 1. In contrast, the mode II stress intensity factor, $\text{Im}(K\,a^{i\varepsilon})$, is only mildly sensitive to the magnitude of $\bar{E}_2/\bar{E}_1$ for all 4 crack tips.

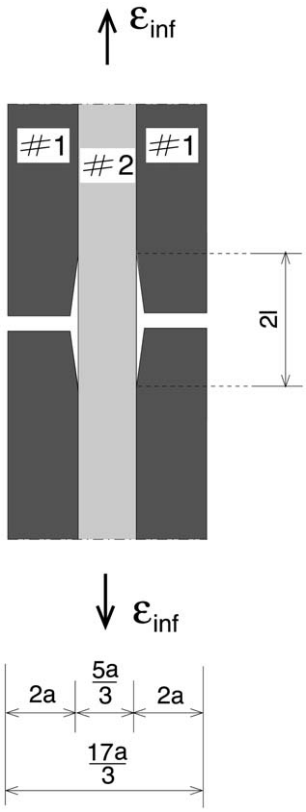

Figure 15. Doubly deflected crack in the two outer layers of a 2/1 lay-up.

Figure 14b shows that the plane strain energy release rate G_d drops monotonically with increasing $\bar{E}_2/\bar{E}_1$, and is consistently the largest for tip 1 near the free surface and the smallest for tip 4 near the centre of the 5/4 lay-up. This implies that *greatest delamination* is expected for the *outermost plies*. The small difference in ψ and G_d for tips 3 and 4 suggests that a uniform delamination state will be achieved in the core region of a very thick multi-layer laminate, with increased delamination of the outermost plies.

5. Effect of number of plies upon failure

5.1. Cracking in a 2/1 lay-up

In order to examine the effect of the number of plies upon failure, the failure mechanisms in the 5/4 lay-up will be compared to those of the 2/1 lay-up depicted in Figure 15. The 2/1 lay-up comprises a layer of material 2 sandwiched between two layers of material 1, and has been regularly applied for the fibre-metal laminates ARALL and GLARE (Marissen, 1988; Vermeeren, 1995; de Vries, 2001). The H-shape crack pattern in the 2/1 lay-up is similar to that in Figure 4b for the 5/4 lay-up, and competing failure modes for the 2/1 lay-up are analysed below. Since the current configuration is thinner than the 5/4 lay-up, the finite element models employed are composed of considerably fewer elements: between 4000 and 5000. For reasons of symmetry, only a quarter of the configuration depicted in Figure 15 has been modelled.

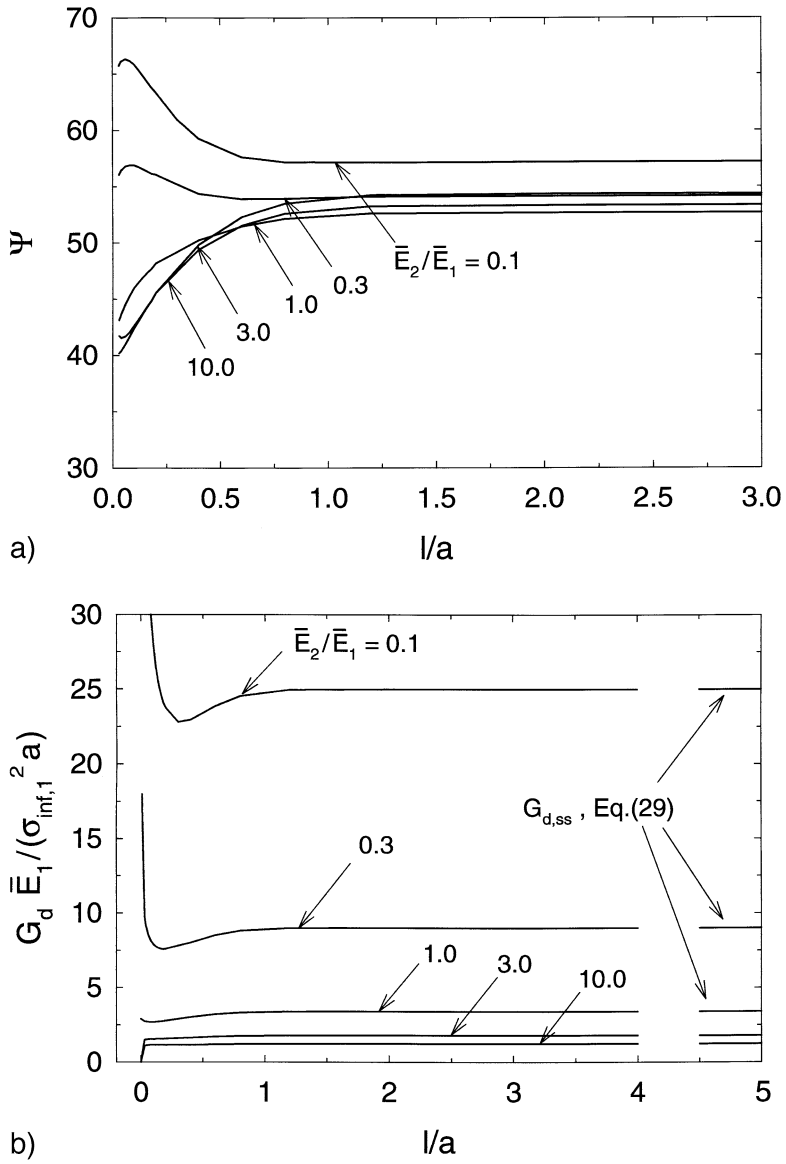

Figure 16. Cracking in the two outer layers of the 2/1 lay-up, see Figure 15. (a) Mode-mixity, $\psi = \text{atan}(\text{Im}(K\,a^{i\epsilon})/\text{Re}(K\,a^{i\epsilon}))$, versus delamination length l/a. (b) Energy release rate for plane-strain delamination G_d versus delamination length l/a.

5.1.1. *Mode-mix and energy release rate*

The mode-mix $\psi(l/a)$ for plane-strain delamination is shown in Figure 16a. For the stiffness ratios considered the steady-state value for the mode-mix lies between 50° and 60°, which is in good agreement with the mode-mix values for the UCSB four-point bend specimen, as derived by Suo and Hutchinson (1990). Further, there is a striking correspondence with the mode-mix for plane-strain delamination of the outermost layers of the 5/4 lay-up, see Figure 10a. Conversely, the energy release rate for plane-strain delamination $G_d(l/a)$ for the 2/1 lay-up, as shown in Figure 16b, is qualitatively different from that for the 5/4 lay-up (Figure 10b): a

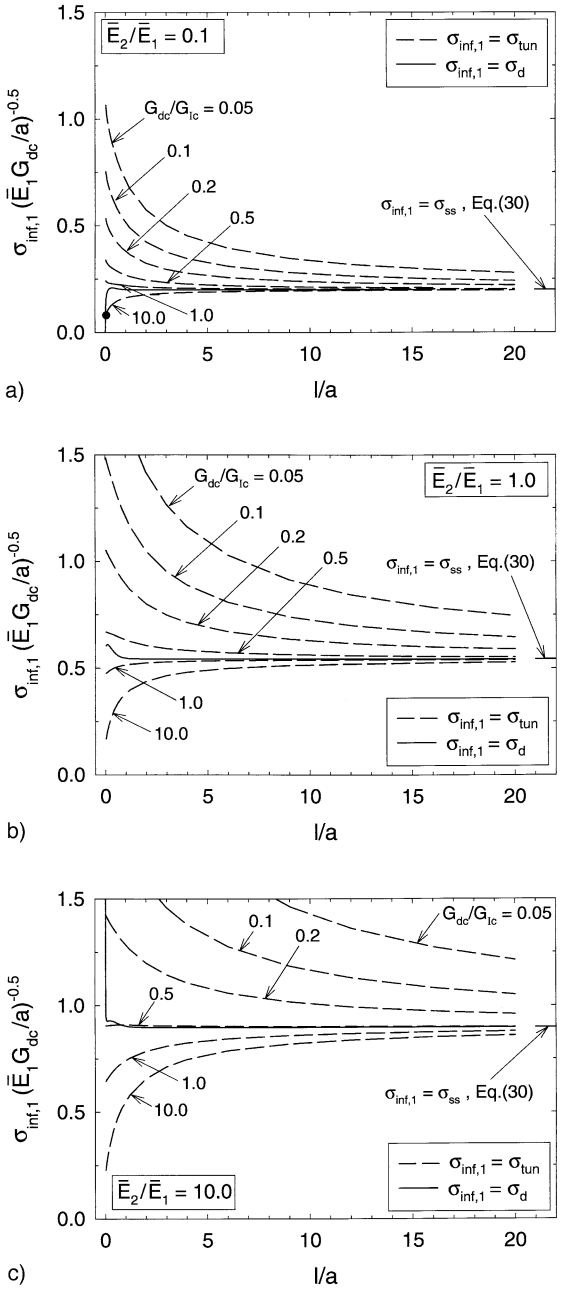

Figure 17. Remote stress $\sigma_{\inf,1}$ versus delamination length l/a (cracking in the two outer layers of the 2/1 lay-up, see Figure 15). Solid line designates the plane-strain delamination curve $\sigma_d - l/a$ and dashed lines designate the (steady-state) tunneling curves $\sigma_{\text{tun}} - l/a$. A black dot indicates the minimum tunneling stress for mechanism 2. (a) $\bar{E}_2/\bar{E}_1 = 0.1$. (b) $\bar{E}_2/\bar{E}_1 = 1.0$. (c) $\bar{E}_2/\bar{E}_1 = 10.0$.

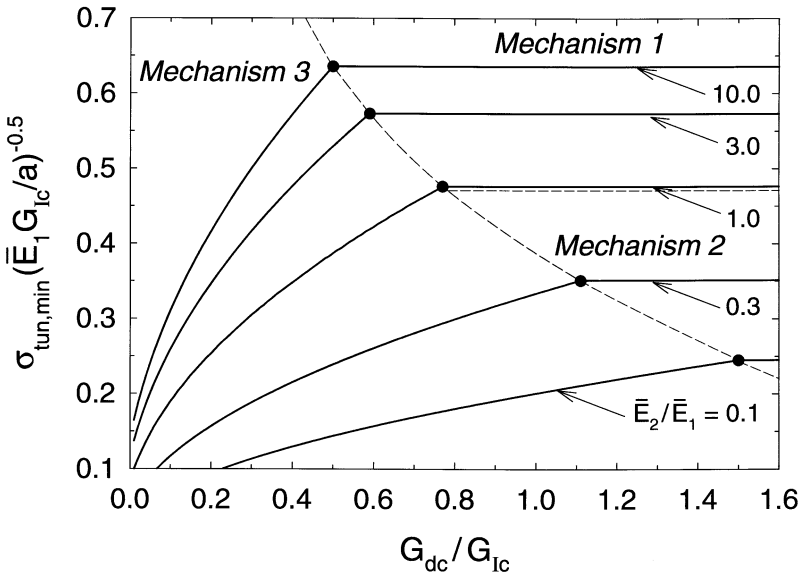

Figure 18. Cracking in the two outer layers of the 2/1 lay-up, see Figure 15. Minimum tunneling stress $\sigma_{\text{tun,min}}$ versus fracture toughness ratio G_{dc}/G_{Ic}. Dashed lines indicate the zones corresponding to the three failure mechanisms in Figure 2.

local minimum in the $G_d(l/a)$ curves is noted for $\bar{E}_2/\bar{E}_1 = 0.1$ and 0.3 in the 2/1 lay-up, but not in the 5/4 lay-up. The steady-state values shown in Figure 16b have been calculated by means of Equation (29), upon substituting $n = 2$, $w_1 = 2a$ and $w_2 = 5a/3$. The numerical predictions converge to the asymptotic values, as expected.

5.1.2. *Failure mechanisms*

The remote delamination stress and the remote tunneling stress for the 2/1 lay-up are plotted against the delamination length in Figures 17a, b and c for $\bar{E}_2/\bar{E}_1 = 0.1$, 1.0, and 10.0, respectively. It is noted that the critical stress levels are lower than those for cracking of the outermost plies of the 5/4 lay-up (Figure 11). For $\bar{E}_2/\bar{E}_1 = 0.1$, stable tunneling of an H-shape crack occurs if $G_{dc}/G_{Ic} > 1.5$ (*mechanism 2* in Figure 2), though it is characterised here by very small delamination lengths, $l/a \ll 1$, see Figure 17a. Alternatively, for $G_{dc}/G_{Ic} \leq 1.5$, *mechanism 3* operates with $\sigma_{\text{tun,min}} = \sigma_{\text{tun}}(l/a \to \infty) = \sigma_{ss}$. Next, consider the case $\bar{E}_2/\bar{E}_1 = 1.0$ shown in Figure 17b: *mechanism 1* is active for $G_{dc}/G_{Ic} > 0.77$ and is replaced by *mechanism 3* for $G_{dc}/G_{Ic} \leq 0.77$. It is clear from Figure 17c that *mechanism 1* is triggered for $G_{dc}/G_{Ic} > 0.5$ and *mechanism 3* operates for $G_{dc}/G_{Ic} \leq 0.5$.

The minimum tunneling stress $\sigma_{\text{tun,min}}$ is plotted against the toughness ratio G_{dc}/G_{Ic} in Figure 18, together with the dominant failure mechanisms for selected values of $\bar{E}_2/\bar{E}_1$. For laminates with a relatively low toughness ratio G_{dc}/G_{Ic} *mechanism 3* prevails. For high toughness ratios *mechanism 1* and *2* dominate, though *mechanism 2* here is characterised by a delamination length very close to zero, see Figure 17a, so it may be difficult to distinguish experimentally this mechanism from *mechanism 1*. This is an important difference with the 5/4 lay-up, where tunneling with constant delamination of a measurable length occurs for a considerable range of toughness ratios G_{dc}/G_{Ic}, especially when the stiffness ratio $\bar{E}_2/\bar{E}_1$ is relatively small, see Figures 9b and 12b.

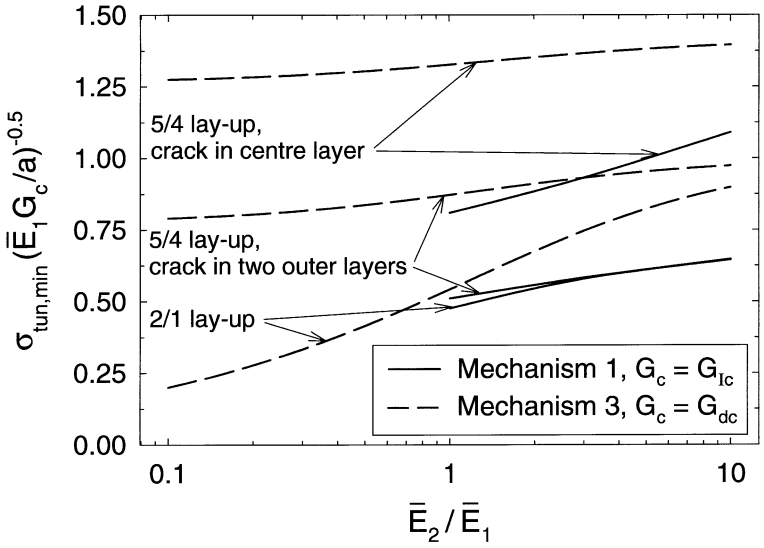

Figure 19. Failure strength $\sigma_{\text{tun,min}}$ versus stiffness ratio $\bar{E}_2/\bar{E}_1$ for mechanisms 1 (solid lines) and 3 (dashed lines).

5.2. Failure strength for mechanisms 1 and 3

It is instructive to depict the failure strength for *mechanisms 1* and *3* as functions of $\bar{E}_2/\bar{E}_1$, see Figure 19. The critical stress for *mechanism 1* is obtained by taking the limit $\sigma_{\text{tun,min}} = \sigma_{\text{tun}}(l/a \to 0)$ from the finite element results. The critical stress for *mechanism 3* is $\sigma_{\text{tun,min}} = \sigma_{\text{tun}}(l/a \to \infty) = \sigma_{ss}$, and is given explicitly by Equation (23) for the central crack and by Equation (30) for the doubly deflected crack in the two outermost plies. Results are given for both the 5/4 lay-up and the 2/1 lay up. The 5/4 lay-up with a crack in the centre layer has the largest failure strength, both for *mechanism 1* and *mechanism 3*, followed by the 5/4 lay-up with a crack in the two outer layers and the 2/1 lay-up (with a crack in the two outer layers). Figure 19 may serve as a design tool provided the failure mechanism is known. However, *mechanism 2* can intervene, depending upon the magnitude of G_{dc}/G_{Ic}, as evidenced by the failure mechanism maps shown in Figures 9a, 12a and 18.

5.3. Steady-state delamination stress for various laminate thicknesses

The steady-state stresses, Equations (23) and (30) for the central H-shape crack and doubly deflected crack in the two outermost layers, respectively, are plotted against the number of plies n of material 1, see Figures 20a, b. The layer widths in Equations (23) and (30) have been taken as $w_1 = 2a$ and $w_2 = 5a/3$. It can be seen that a higher stiffness ratio results in a higher steady-state (residual) delamination strength. For relatively small stiffness ratios the steady-state stress initially increases sharply with increasing n, especially for the case of a doubly deflected crack in the two outermost layers. For relatively thick laminates, $n > 5$, a significant change of the stiffness ratio $\bar{E}_2/\bar{E}_1$ produces only a small change in the steady-state stress σ_{ss} (= failure strength for *mechanism 3*).

6. Comparison with experiments

The practical applicability of the expressions for the steady-state stress, Equations (23) and (30), is demonstrated by means of a comparison with the experiments reported in de Vries et al. (1999). In these experiments the delamination behaviour of a GLARE 3/2 laminate (3 aluminium layers and 2 glass-fibre/epoxy layers) was examined, by considering an H-shape crack in the centre layer of the specimen and a doubly deflected crack in the two outermost layers of the specimen. The pre-cracked configurations were similar to those depicted in Figure 4 for the 5/4 lay-up but without initial delaminations. Accordingly, the fracture energy released during the experiment was fully due to delamination. Three different thicknesses for the aluminium layers were considered: $w_1 = 0.2$ mm, 0.3 mm and 0.5 mm. The thickness of the fibre/epoxy layers was equal to $w_2 = 0.125$ mm. The axial stiffness of the aluminium layers was $E_1 = 72$ GPa, and the stiffness moduli for the fibre/epoxy layers were $E_{2l} = 54$ GPa in the direction parallel to the fibre orientation and $E_{2t} = 9.4$ GPa in the transverse direction. In the current comparison, only those configurations are considered for which the fibres are oriented in the loading direction (i.e. $E_2 = 54$ GPa).

The gross failure stress is given in Table 1 for various thicknesses of the aluminium layer. The steady-state stress in the aluminium (material 1) has been computed by means of Equations (23) and (30), using a delamination toughness $G_{dc} = 0.6$ N mm^{-1}. The stress in the fibre layers (material 2), follows from the compatibility requirement $\sigma_{\text{inf},1}/E_1 = \sigma_{\text{inf},2}/E_2$, and the gross failure stress is the weighted average over the total thickness of the laminate. Table 1 shows that the comparison between the experimental results and the model predictions is reasonably good. Both the experiments and the model give a lower gross failure stress for a thicker aluminium layer. The reason for this is that a thicker aluminium layer behaves in a stiffer manner, and produces a higher stress intensity at the delamination tips. The maximum discrepancy between the predicted and measured strengths equals 19%, which may be due to effects that have not been incorporated in the model, such as yielding of the aluminium, anisotropy of the fibres and residual stresses as a result of the manufacturing process. Despite these deficiencies, the comparison confirms that Equations (23) and (30) provide reasonably accurate estimates for the residual failure strength of the laminate.

7. Concluding remarks

Steady-state crack tunneling and plane-strain delamination have been investigated in laminates subjected to a remote uniform tensile strain. Three mechanisms have been distinguished: (i) tunneling of a mode I crack without delamination, (ii) tunneling of an H-shape crack with constant delamination length, and (iii) unstable delamination growth in all directions. For each of these mechanisms the critical stress is taken as the minimum tunneling stress. The minimum tunneling stress of the laminate is dependent upon the delamination toughness at the layer interfaces and upon the stiffness ratio of the layers. The dependence of the tunneling stress upon the crack location and the number of plies within the laminate has also been explored. Closed form expressions for the steady-state stress have been obtained, and may be useful in design against delamination.

To further investigate the phenomena discussed in this paper, more systematic experimental studies are necessary, both in regards to the static and the fatigue behaviour of laminate structures. The sensitivity of the above results to material anisotropy and plasticity effects are also topics for future study.

Table 1. Comparison of the gross failure strength of a GLARE 3/2 laminate, as determined experimentally (de Vries et al., 1999), and calculated via Equation (23) (H-crack in centre layer of laminate) and Equation (30) (Doubly deflected crack in two outer layers of laminate)

Thickness aluminium layer	$w_1 = 0.5$ mm			$w_1 = 0.3$ mm			$w_1 = 0.2$ mm		
	Measured gross failure strength	Calculated gross failure strength	Relative difference	Measured gross failure strength	Calculated gross failure strength	Relative difference	Measured gross failure strength	Calculated gross failure strength	Relative difference
H-crack centre layer	432 N mm^{-2}	476 N mm^{-2}	10.2%	613 N mm^{-2}	611 N mm^{-2}	0.3%	855 N mm^{-2}	744 N mm^{-2}	13.0%
Defl. crack two outer layers	244 N mm^{-2}	256 N mm^{-2}	4.9%	353 N mm^{-2}	340 N mm^{-2}	3.7%	530 N mm^{-2}	427 N mm^{-2}	19.4%

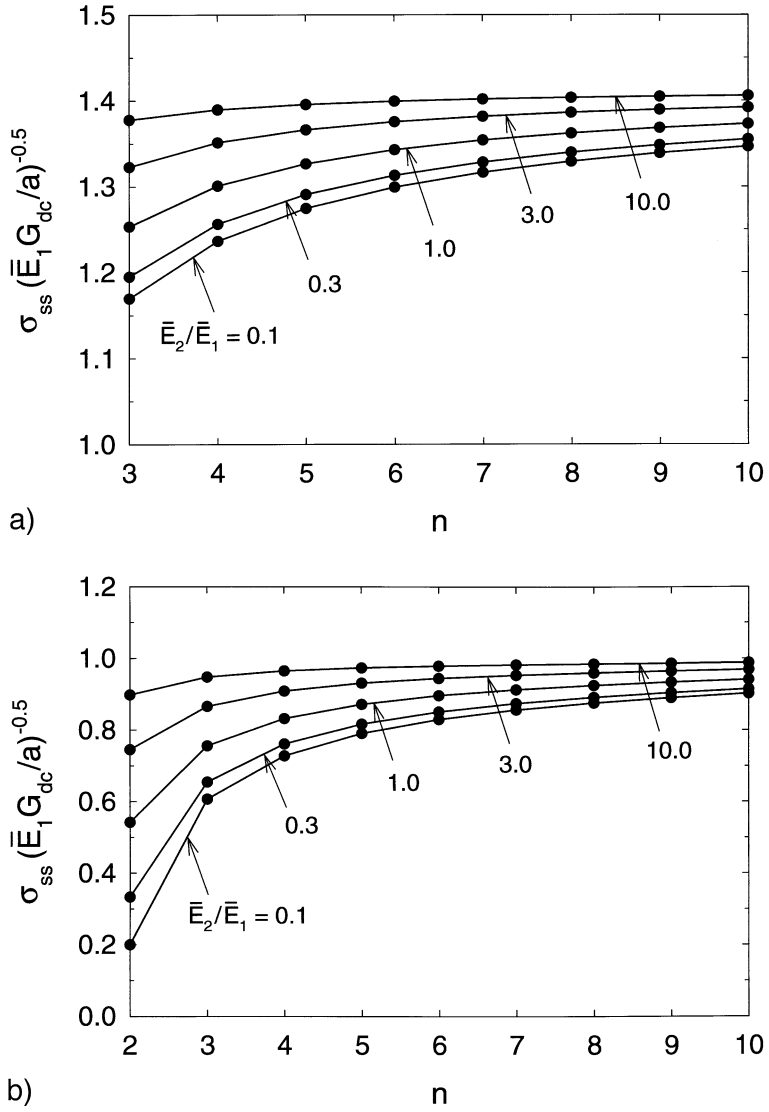

Figure 20. Steady-state stress for plane-strain delamination σ_{ss} versus laminate thickness (n = number of plies of material 1). (a) H-shape crack in the centre layer of the laminate, Equation (23). (b) Doubly deflected crack in the two outer layers of the laminate, Equation (30).

Acknowledgements

The helpful discussions with Dr Tian Jian Lu are appreciated by the authors. A.S.J.S. is grateful for the hospitality offered by the Cambridge Centre for Micromechanics at the Cambridge University, Cambridge, United Kingdom, during an eight month leave from the Delft University of Technology, Delft, The Netherlands. Both authors are grateful for EU support in the form of TMR and RTN grants ERB-4061-PL-95-0988 and HPRN-CT-2002-00198.

References

Beuth, J.L. (1992). Cracking of thin bonded films in residual tension. *Int. J. Solids Struct.* **29**, 1657–1675.

Broek, D. (1986). *Elementary Engineering Fracture Mechanics*, Martinus Nijhoff Publishers, Dordrecht.

Chan, K.S., He, M.Y. and Hutchinson, J.W. (1993). Cracking and stress redistribution in ceramic layered composites. *Mat. Sci. Engrg.* **A167**, 57–64.

Cox, B.N. and Marshall, D.B. (1996). Crack initiation in fiber-reinforced brittle laminates, *J. Am. Ceram. Soc.* **79**, 1181–1188.

de Vries, T.J. (2001). *Blunt and Sharp Notch behaviour of Glare Laminates*. Dissertation, Delft University of Technology, The Netherlands.

de Vries, T.J., Vlot, A. and Hashagen, F. (1999). Delamination behavior of spliced Fiber Metal Laminates. Part 1. Experimental results. *Compos. Struct.* **46**, 131–145.

Dollar, A. and Steif, P.S. (1991a). The branched crack problem revisited. *J. Appl. Mech. (ASME)* **58**, 584–586.

Dollar, A. and Steif, P.S. (1991b). Stresses in fibers spanning an infinite matrix crack. *Int. J. Solids Struct.* **27**, 1011–1024.

Dundurs, J. (1969). Edge-bonded dissimilar orthogonal elastic wedges. *J. Appl. Mech. (ASME)* **36**, 650–652.

Dvorak, G.J. and Laws, N. (1986). Analysis of first ply failure in composite laminates. *Engrg. Frac. Mech.* **25**, 763–770.

Fleck, N.A. and Zhao, L.G. (2000). Microbuckle tunnelling in fibre composites. *J. Mech. Phys. Solids* **48**, 1865–1891.

He, M-Y., Evans, A.G. and Hutchinson, J.W. (1994). Crack deflection at an interface between dissimilar elastic materials: role of residual stresses. *Int. J. Solids Struct.* **31**, 3443–3455.

He, M.-Y. and Hutchinson, J.W. (1989). Crack deflection at an interface between dissimilar elastic materials. *Int. J. Solids Struct.* **25**, 1053–1067.

Ho, S. and Suo, Z. (1993). Tunneling cracks in constrained layers. *J. Appl. Mech. (ASME)* **60**, 890–894.

Hutchinson, J.W. and Lu, T.J. (1995). Laminate delamination due to thermal gradients. *J. Engrg. Mat. Tech. (ASME)* **117**, 386–390.

Hutchinson, J.W., Mear, M. and Rice, J. (1987). Crack paralleling an interface between dissimilar materials. *J. Appl. Mech. (ASME)* **54**, 828–832.

Hutchinson, J.W. and Suo, Z. (1992). Mixed mode cracking in layered materials. *Adv. Appl. Mech.* **29**, 63–191.

Li, F.Z., Shih, C.F. and Needleman, A. (1985). A comparison of methods for calculating energy release rates. *Engrg. Frac. Mech.* **21**, 405–421.

Liechti, K.M. and Chai, Y.-S. (1992). Asymmetric shielding in interfacial fracture under in-plane shear. *J. Appl. Mech. (ASME)* **59**, 295–304.

Lu, T.J. (1996). Crack branching in all-oxide ceramic composites. *J. Am. Ceram. Soc.* **79**, 266–274.

Marissen, R. (1988). *Fatigue crack growth in ARALL- A hybrid aluminium-aramid composite material*, Dissertation, Delft University of Technology, The Netherlands.

Matos, P.P.L., McMeeking, R.M., Charalambides, P.G. and Drory, M.D. (1989). A method for calculating stress intensities in bimaterial fracture. *Int. J. Frac.* **40**, 235–254.

Parks, D.M. (1974). A stiffness derivative finite element technique for determination of crack tip stress intensity factors. *Int. J. Frac.* **10**, 487–501.

Rice, J.R. (1968). A path-independent integral and approximation analysis of strain concentration by notches and cracks. *J. Appl. Mech. (ASME)* **35**, 379–386.

Rice, J.R. (1988). Elastic fracture concepts for interfacial cracks. *J. Appl. Mech. (ASME)* **55**, 98–103.

Suo, Z. and Hutchinson, J.W. (1990). Interface crack between two elastic layers. *Int. J. Frac.* **43**, 1–18.

Takamatsu, T., Matsumura, T., Ogura, N., Shimokawa, T. and Kakatu, Y. (1999). Fatigue crack growth properties of a GLARE-3-5/4 fiber/metal laminate. *Engrg. Frac. Mech.* **63**, 253–272.

Takamatsu, T., Shimokawa, T. and Matsumura, T. (2001). Application of a compliance method to fatigue crack growth analysis of GLARE-3 fiber-metal laminates. *21st Symposium of the International Committee on Aeronautical Fatigue, Toulouse, France*. 1–17.

Vermeeren, C.A.J.R. (1995). *The Residual Strength of Fibre Metal laminates*. Dissertation, Delft University of Technology, The Netherlands.

Vlot, A. and Gunnink, J.W. (eds.) (2001). *Fibre Metal Laminates - An Introduction*. Kluwer Academic Publishers, Dordrecht.

Vlot, A., Vogelesang, L.B. and de Vries, T.J. (1999). Towards application of fibre metal laminates in large aircraft. *Aircraft Engrg. Aerosp. Tech.* **71**, 558–570.

Vogelesang, L.B., Schijve, J. and Fredell, R. (1995). Fibre-metal laminates: damage tolerant aerospace materials, *Case studies in Manufacturing with Advanced Materials*, Demaid A., de Wit J.H.W., Eds., volume 2. Elsevier, Amsterdam.

Ye, T., Suo, Z. and Evans, A.G. (1992). Thin film cracking and the roles of substrate and interface. *Int. J. Solids Struct.* **29**, 2639–2648.